



## Research article

Stability, spectroscopic, electrochemistry and QTAIM analysis of Cu-Zn<sub>n-1</sub>O<sub>n</sub> clusters for glucose sensing application: A study on theoretical and experimental insightsB. Gassoumi<sup>a,\*</sup>, N. Aouled Dlala<sup>b</sup>, M. Echabaane<sup>a,c</sup>, A. Karayel<sup>d,\*\*</sup>, S. Özkınalı<sup>e</sup>, M.E. Castro<sup>f</sup>, F.J. Melendez<sup>g</sup>, H. Ghalla<sup>b</sup>, L. Nouar<sup>h</sup>, F. Madi<sup>h</sup>, R. Ben. Chaabane<sup>a,\*\*\*</sup><sup>a</sup> Laboratory of Advanced Materials and Interfaces (LIMA), University of Monastir, Faculty of Science of Monastir, Avenue of Environment, 5000 Monastir, Tunisia<sup>b</sup> Quantum and Statistical Physics Laboratory, Faculty of Sciences, University of Monastir, 5079 Monastir, Tunisia<sup>c</sup> NANOMISENE Lab, LR16CRMN01, Centre for Research on Microelectronics and Nanotechnology CRMN of Technopark of Sousse, B.P. 334, Sahloul, 4034 Sousse, Tunisia<sup>d</sup> Department of Physics, Faculty of Arts and Sciences, Hitit University, Çorum, Turkey<sup>e</sup> Department of Chemistry, Faculty of Arts and Sciences, Hitit University, Çorum, Turkey<sup>f</sup> Centro de Química del Instituto de Ciencias, Benemérita Universidad Autónoma de Puebla, 18 sur y Av. San, Claudio, Col. San Manuel Puebla C. P. 72570, Mexico<sup>g</sup> Lab. de Química Teórica, Centro de Investigación, Depto. de Físicoquímica, Facultad de Ciencias Químicas, Benemérita Universidad Autónoma de Puebla, Edif. FCQ10, 22 Sur y San Claudio, Ciudad Universitaria, Col. San Manuel, C.P 72570, Puebla, Mexico<sup>h</sup> Laboratory of Computational Chemistry and Nanostructures, Department of Material Sciences, Faculty of Mathematical, Informatics and Material Sciences, University of 8 May 1945, Guelma, Algeria

## ARTICLE INFO

## Keywords:

ZnO  
MEP  
Acceptors sites  
Charge transfer  
QTAIM  
DFT-D3

## ABSTRACT

Clusters of (ZnO)<sub>n</sub> (n = 2–4) have been shown to play a central role in the detection of glucose entity based on the existence of photo-induced electrons (PE), which facilitates the interaction between (ZnO)<sub>n</sub> clusters and glucose entity guests. The electrochemistry experiment has confirmed the detection of glucose by the title clusters. The optimization, energetic parameters, and vibrational frequency calculations have indicated that the Cu-Zn<sub>n-1</sub>O<sub>n</sub>-glucose are more stable than the (ZnO)<sub>n</sub>-glucose complexes. It has been demonstrated that the Cu doping enhanced the chemical behavior of the clusters and formed a high intramolecular charge transfer (ICT) in the system. The glucose sensing by all the forms of Cu-Zn<sub>n-1</sub>O<sub>n</sub> clusters showed that the Cu-Zn<sub>3</sub>O<sub>4</sub>, Cu-Wurtzite, and Cu-Rocksalt clusters are the most suitable for adsorbing the glucose guest. The HOMO/LUMO iso-surfaces of the complexes showed that the electron concentrations are localized in the d orbitals and mainly in the form of the d<sup>10</sup> orbitals around Zn atoms. The molecular electrostatic potential (MEP) has clearly indicated that a high charge transfer occurs between the copper and the oxygen atoms, which facilitate the adsorption of glucose. The reactivity parameters also indicated that the Wurtzite-glucose complex has a high electrophilicity index (ω), which means a good acceptor behavior to interact with glucose. Additionally, the bond between the (ZnO)<sub>n</sub> clusters and the glucose polar element has been studied in detail by using QTAIM theory. Finally, the theoretical and experimental studies prove that the Cu-Zn<sub>n-1</sub>O<sub>n</sub> clusters are very suitable and competent compounds for detecting glucose.

## 1. Introduction

Nanomedicine is an area based on the use of new powerful technologies for the treatment of human diseases [1, 2, 3, 4]. The clustering behavior arising from their small size gives birth to using these entities

instead of proteins and biomolecules in human cells against specific diseases [5, 6, 7, 8, 9]. The clusters (for example, ZnS, CdS, CdSe, etc.) have a beneficial characteristic; they can alter their morphological, magnetic, and chemical properties in interaction with biomolecular systems [10, 11, 12, 13, 14, 15]. Also, the clusters are reorganized by

\* Corresponding author.

\*\* Corresponding author.

\*\*\* Corresponding author.

E-mail addresses: [gassoumibouid2016@gmail.com](mailto:gassoumibouid2016@gmail.com) (B. Gassoumi), [arzukarayel@hitit.edu.tr](mailto:arzukarayel@hitit.edu.tr) (A. Karayel), [rafik.benchaabane@fsm.rnu.tn](mailto:rafik.benchaabane@fsm.rnu.tn) (R. Ben. Chaabane).

well-defined structures and specified by a precise quantum confinement's model [16, 17]. Therefore, the variation of the sizes of the structures of the clusters regulates the efficiency of the opto-electronic behavior of the compounds [18, 19]. ZnO is a non-toxic semiconductor material. ZnO is preferred to bind with nitrogen N atoms, which have three lone electron pairs free to form other bonds. Among them,  $(\text{ZnO})_n$  clusters continue attracting the attention of physicists, chemists, and doctors to use them in several applications because of their high exciton binding energy (60 meV), wide band gap, and cost effective synthesis methods [20, 21, 22]. The ZnO material can be used in a variety of applications, such as photo detectors [23], antibacterial activity [24], adsorption of polluting gases [25], and environmental sensors [26]. All these advantages are defined in the pure ZnO material, but now, we have focused on the Cu doping of  $(\text{ZnO})_n$ . The  $\text{Cu}^{2+}$  cation is of the  $sp^2$  latent positive type on the nanoscale. Its properties are important factors that enhance the electronic properties of  $(\text{ZnO})_n$ . The doping of such a copper cation is an efficient way to obtain a good glucose sensor (there are two electron-hole pairs due to the presence of this ion in ZnO). It is important to mention that the majority of the reported studies have done experimental analyses, but a good explication of the adsorption and chemical sensing processes for all the possible configurations of ZnO to glucose has not yet been reported [27, 28, 29, 30]. Recently, the enzymatic and non-enzymatic electrochemical [31], neuron fibers [32], nitrogen-doped graphene quantum dots [33], and plasmonic [34] systems have been experimentally tested for glucose sensing in the literature. Also, theoretically, the CDs nanoparticles [35], boronic acid decorated graphene nanoflakes [36], nanocages [37] are complexed with the glucose entity for adsorption application. In our paper, we have turned to other interesting sensor systems (ZnO clusters). In this work, the interaction mechanism between the  $(\text{ZnO})_n$  before and after Cu doping, and glucose is studied and visualized for understanding the interactions and forces stabilizing the complexes and the chemical groups that favor the donor-acceptor process during the adsorption.

The  $(\text{ZnO})_n$  and  $\text{Cu-Zn}_{n-1}\text{O}_n$  compounds were synthesized, and the morphological characterization was studied using the TEM and XRD analyses. The calculation of the energetic and structural parameters using the B3LYP-D3/Lanl2DZ method shows that the  $\text{Cu-Zn}_3\text{O}_4$  systems for the ring, rocksalt, and wurtzite forms are more stable in comparison with the other clusters. The vibrational modes of the most stable systems after Cu doping confirmed the stability of the clusters. The theoretical FT-IR study was done in detail to understand the dynamic stability of the  $\text{Cu-Zn}_{n-1}\text{O}_n$ -glucose complexes. From HOMO/LUMO and MEP plots, it is indicated that the doping Cu reinforces the appearance of an intra-atomic charge transfer. The electronic properties and the chemical reactivity parameters have demonstrated that the doping clusters ( $\text{Cu-Zn}_3\text{O}_4$ -

glucose, Cu-Wurtzite-glucose, and Cu-Rocksalt-glucose) are more suitable to adsorb glucose entities more than the non-doping ones. Bader's analysis indicated that the glucose is stabilized with  $\text{Cu-Zn}_{n-1}\text{O}_n$  by hydrogen bonding interactions. The electrochemical analyses confirmed the detection of the glucose by  $\text{Cu-Zn}_{n-1}\text{O}_n$  clusters.

## 2. Experimental method

### 2.1. Preparation of doped $\text{Cu-ZnO}_n$ clusters

The synthetic pathway to obtain the ZnO and the Cu-ZnO compounds is described by Omri et al. [38]. These materials were prepared by the sol-gel process under supercritical conditions in ethyl alcohol (EtOH). The molecular structure of the single  $\text{Zn}_2\text{O}_2$  compound is given in Figure 1 (molecular geometry (a), compact model (b) and 2D chemical structure(c)).

### 2.2. TEM and XRD characterizations

The ZnO and Cu-ZnO clusters were characterized by XRD and TEM (Figure 2). It is shown from the XRD diagrams (see Figure 2c) of the ZnO and Cu-ZnO clusters that there appears a sharp and intense diffraction peak, which proves the high crystalline nature of the samples. No peaks of impurities can be detected, indicating that the product ZnO has a pure structure. The absence of Cu-related phase diffraction peaks indicated that the  $\text{Cu}^{2+}$  ions have replaced the  $\text{Zn}^{2+}$  ions without modifying the lattice crystal structure. Furthermore, it is clearly observed for the non-doped ZnO that the diffraction intensities of all the peaks are higher; this result indicates that the incorporation of Cu dopants increases the crystallographic defects in the ZnO structure and therefore degrades the crystal quality. Accurate 3D graphs by TEM characterization for ZnO and Cu-ZnO samples have been investigated (see Figure 2(a)-(b)). From the micrographs, it is observed that the non-doped ZnO is composed of large aggregates, indicating that the ZnO clusters grew at a high density. It is found that these clusters exhibit a spherical shape with a narrow size distribution. In addition, Cu-ZnO clusters are observed to have a clear change in the surface morphology. According to the TEM findings, the average cluster size of the ZnO is about 35 nm, and the Cu-ZnO is found at 46 nm. Finally, the growths of the ZnO samples tend to develop segregation according to the revitalization of the Cu substitutions.

## 3. Computational methodology

The density functional theory with dispersion correction method (DFT-D3) [39,40] was performed to find steady states of the complexes

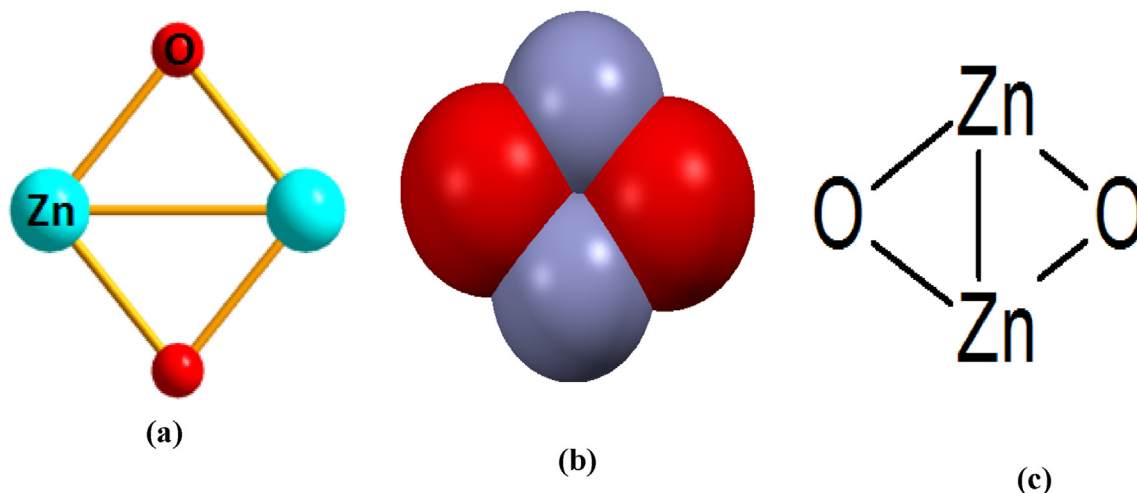
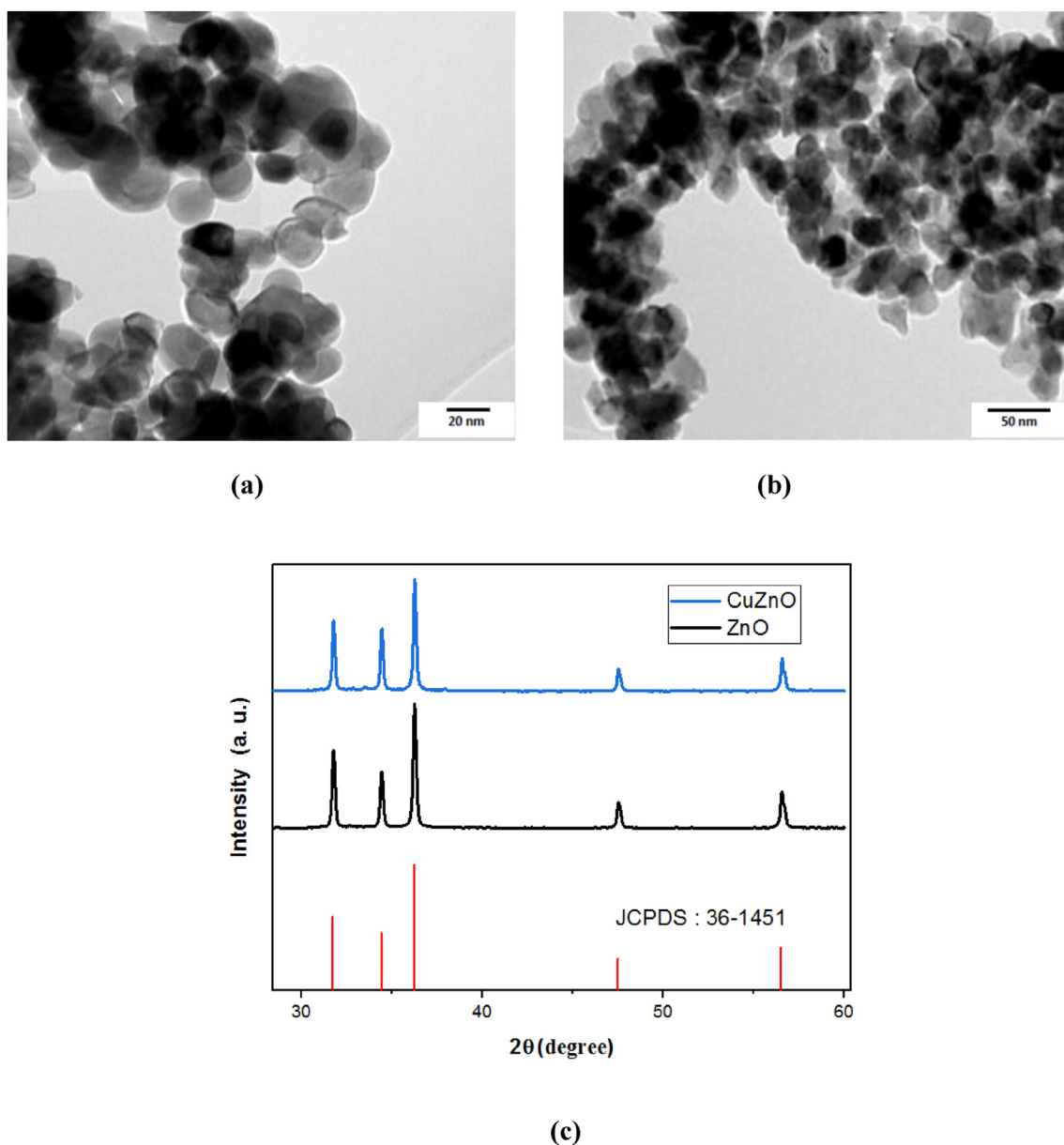


Figure 1. (a): Molecular geometry, (b): Compact representation and, (c): the chemical structure of the  $\text{Zn}_2\text{O}_2$  compound.



**Figure 2.** (a) and (b): TEM characterization, and (c): X-ray diffraction analysis of ZnO and Cu–ZnO cluster.

and to examine the electronic properties of the compounds. The DFT-D3 was carried out using the Gaussian 09 software [41], and the results were visualized with the GaussView 5.0 program [42]. The stability and energy parameters of the clusters before complexation are discussed.  $(\text{ZnO})_n$  and  $\text{Cu-Zn}_{n-1}\text{O}_n$  structures for  $n = 2-4$  were proved to interact with glucose in three different positions named pos1, pos2, and pos3, shown in Figure 3. Complexes were calculated using the B3LYP-D3 [43] method with 6-311G(d,p) and the LanL2DZ-D3 [44] basis set. The  $(\text{ZnO})_n$  and  $\text{Cu-Zn}_{n-1}\text{O}_n$  clusters geometries for  $n = 2-4$  after optimization stage of the complexes were compared in detail with their initial geometries. The minimized structures of these complexes are shown in Figure 3. The optimized geometries of all structures correspond to the true global minima since no imaginary frequencies were observed in the vibrational frequency investigation. The optimization energies are listed in Table 2 and minimum energies are boldly highlighted. The chemical reactivity and the possible charge transfer phenomenon in each compound, passing from  $n = 2-4$  before complexation, are examined by the molecular orbital analysis. The nucleophilicity and hydrophobicity of these compounds are studied by MEP-MK analysis at the same level of theory. The

band gap energies, ionization potential, electron affinity, electronegativity, chemical hardness, chemical softness, chemical potential, and electrophilic index were calculated from the HOMO and LUMO energies. The nature and type of interaction in all the active sites between the  $(\text{ZnO})_n$  and the  $\text{Cu-Zn}_{n-1}\text{O}_n$  clusters, and the glucose have been interpreted via the QTAIM theory [45]. The topological parameters have been carried out by using the Multiwfn package [46].

## 4. Results and discussion

### 4.1. Stability and energetic analyses of $\text{Zn}_n\text{O}_n/\text{Cu-Zn}_{n-1}\text{O}_n$ clusters

The optimized structures of the  $(\text{ZnO})_n$  clusters, such as  $(\text{ZnO})_2$ ,  $(\text{ZnO})_3$ ,  $(\text{ZnO})_4$  (R for rocksalt), and  $(\text{ZnO})_4$  (W for wurtzite), have been calculated using two different methods: B3LYP-D3/6-311G(d,p) and B3LYP-D3/LanL2DZ level of theory. The structural parameters (distances (Å) and angles (°)) are indicated on each Figure (see Figure 3a). The calculated parameters are compared with those in the literature [47, 48, 49, 50, 51]. The relaxation energies (in a.u.) correlated to the dipole

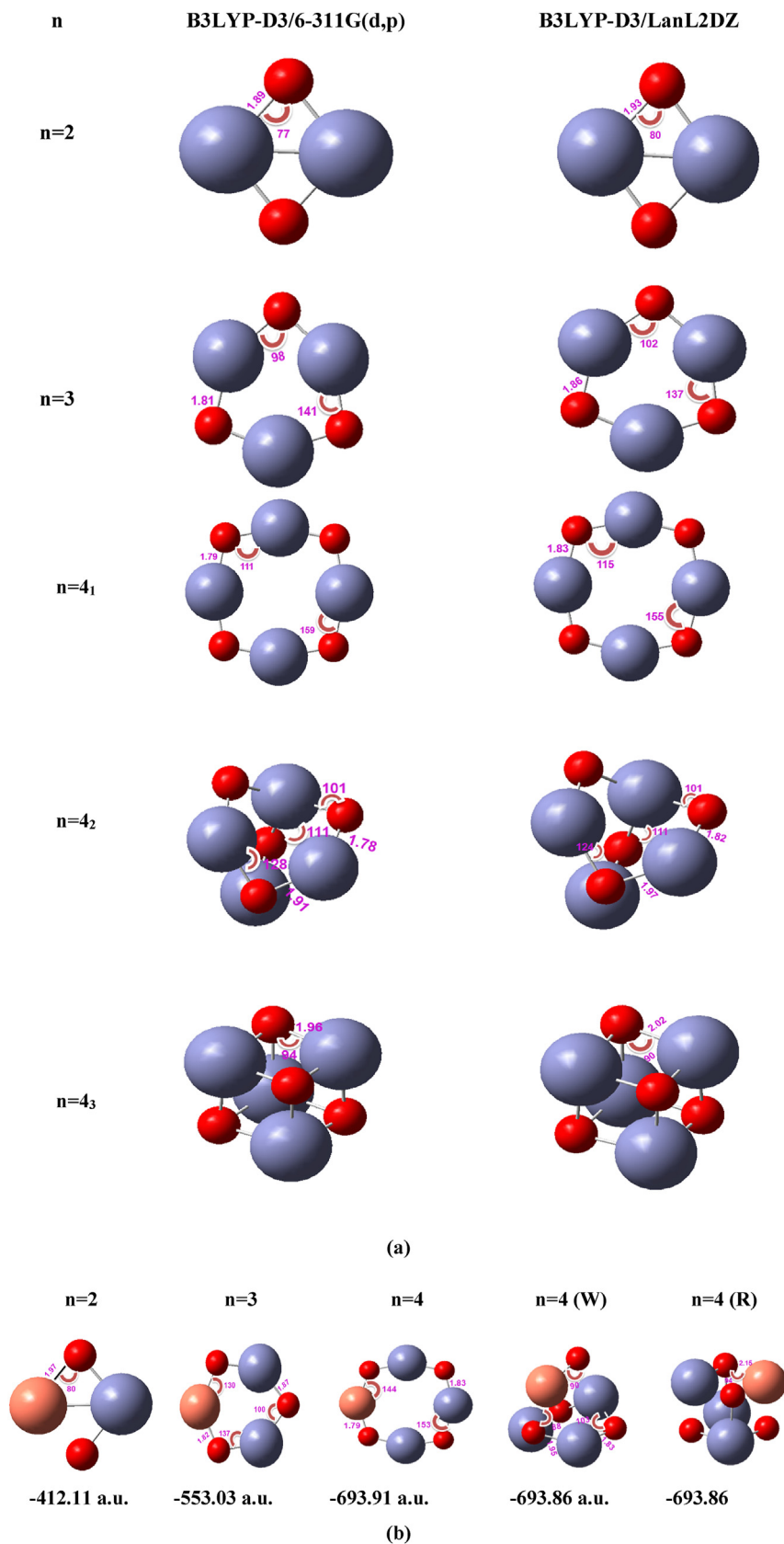


Figure 3. Stable structures of  $(ZnO)_n$  (a), and  $Cu-(Zn_{n-1}O_n)$  clusters.

moment (in Debye) are summarized in Table 1. It is shown that the Zn–O contact is 1.89 Å using the 6-311G(d,p) and 1.93 Å calculated with the LanL2DZ basis sets. The Zn–O–Zn angles calculated by the two methods are equal to 77 and 80°, respectively. The symmetry group is  $C_1$ . The experimental values of the bond length and valence angle are 1.92 Å and 81°, respectively. It was found that the values obtained with the LanL2DZ basis set are close to the experimental results [47]. For  $(ZnO)_3$ , it is obtained that the Zn is distant from O by 1.81 Å (6-311G(d,p)) and 1.86 Å (LanL2DZ), respectively. At the 6-311G(d,p) basis set, the values of the angles Zn–O–Zn are around 98, and 141°, while using the LanL2DZ basis set, the angle values are 102°, and 137°, respectively. It is obtained that the distances between Zn and O are in the range of 1.79 and 1.83 Å, calculated by the two methods. The valence angles are in the range of 111°–159°. It indicates that the symmetry group is Cs. Concerning the wurtzite shape of the  $(ZnO)_4$  cluster, it is found that the Zn–O distances are equal to 1.78 and 1.91 Å calculated by 6-311G(d,p), and 1.82 and 1.92 Å using the LanL2DZ basis set. The valence angles calculated by the two methods are almost the same, with values at 101°, 111°, and 128°, respectively. For the rocksalt cluster, it is clearly observed that the structural parameters are very close. A shift of 4 Å between the Zn and O atoms is found, and the angles are shifted only by 0.06°. The experimental results show that the Zn–O distance is on the order of 1.94 Å and the Zn–O–Zn angle is around 96° [48]. This analysis proves that the second method (B3LYP-D3/LanL2DZ) produces results very close to the experimental ones. Based on the theoretical parameters compared to the experimental values, the B3LYP-D3/LanL2DZ method is more accurate for the energetic study of the clusters. In Table 1, it is shown that the total energy of the studied systems varies from –270.95 a.u. ( $(ZnO)_2$ ) to –521.12 a.u. ( $(ZnO)_{4-pos.3}$ ).

For B3LYP-D3/6-311G(d,p), it is remarkably evident that the systems  $(ZnO)_4$  are more stable than the other clusters. This result is well verified by the low dipole moment values observed for these compounds. It is demonstrated that the system is energetically enhanced when the Zn–O groups are added. The total energy calculated at the B3LYP-D3/LanL2DZ level of theory for the ZnO clusters is around –563 a.u. for the  $(ZnO)_4$  complexes. The values of the dipole moments are equal to 0.004 Debye. The energetic analysis confirmed that the B3LYP-D3/LanL2DZ gave the most stable clusters. In Table 1, it is also shown that the rotational constant (RC/A) values of the three stable systems present the lowest values, proving that these clusters have the most stable kinetic energy, and are therefore the most stable clusters. The values of RC/A vary from 0.60 to 0.85 a.u. Considering the structural and energetic interpretations in comparison with the experimental studies, it is concluded that B3LYP-D3/LanL2DZ is the suitable method to study the doping clusters. The doped  $(ZnO)_n$  systems are shown in Figure 3b. Herein, the compound  $(ZnO)_2$  doped Cu has an O–Cu distance equal to 1.97 Å and the Zn–O–Cu angle is approximately 80°. In comparison with the two systems  $(ZnO)_2$  before and after doping, it is observed that the metal Cu disturbs the system for stabilization. Cu–ZnO<sub>2</sub> has an energy value of around –412.11 a.u. There is a charge transfer phenomenon taking place during doping, which it is explained by the breaking of the bonds between the cation and the nearby atom. All the valence electrons are localized surrounding the

**Table 1.** Total energies  $E_T$  (in a.u.), dipole moment  $\mu$  (in Debye), and the rotational constants RC (in GHz) of the  $(ZnO)_{n=2-4}$  clusters using the different basis sets.

Structure	B3LYP-D3/6-311G(d,p)			B3LYP-D3/LanL2DZ		
	$E_T$	RC/A	M	$E_T$	RC/A	M
$(ZnO)_{n=2}$	–270.95	7.23	0.01	–281.57	7.23	0.008
$(ZnO)_{n=3}$	–403.58	1.54	0.02	–422.49	1.54	0.016
$(ZnO)_{n=4-1}$	–521.19	0.60	0.003	–563.38	0.60	0.003
$(ZnO)_{n=4-2}$	–521.08	0.81	0.004	–563.30	0.81	0.004
$(ZnO)_{n=4-3}$	–521.12	0.85	0.004	–563.36	0.85	0.004

**Table 2.** The optimization energies (in a.u.) of  $(ZnO)_n$ -glucose and Cu- $Zn_{n-1}O_n$ -glucose complexes for  $n = 2-4$  at the B3LYP-D3/LanL2DZ level of theory. Wurtzite (W) and Rocksalt (R) structures are isomers of  $Zn_4O_4$ .

Complex (1–2)	Positions	Zn <sub>2</sub> O <sub>2</sub> -glucose	Cu–Zn <sub>2</sub> O <sub>2</sub> -glucose
	Pos1	–968.7904752	–1099.3310759
	Pos2	–968.8593631	–1099.3235732
	Pos3	–968.8284332	–1099.35427
Complex (3–4)		Zn <sub>3</sub> O <sub>3</sub> -glucose	Cu–Zn <sub>3</sub> O <sub>3</sub> -glucose
	Pos1	–1109.6991483	–1240.195328
	Pos2	–1109.6949069	–1240.2138359
	Pos3	–1109.723559	–1240.2197666
Complex (5–6)		Zn <sub>4</sub> O <sub>4</sub> -glucose	Cu–Zn <sub>4</sub> O <sub>4</sub> -glucose
	Pos1	–1250.5874469	–1381.103446
	Pos2	–1250.5846408	–1381.1409701
	Pos3	–1250.6024025	–1381.1029298
Complex (7–8)		Wurtzite-glucose	Cu–Wurtzite-glucose
	Pos1	–1250.578372	–1381.1007473
	Pos2	–1250.6707559	–1381.162543
	Pos3	–1250.612641	–1381.1807028
Complex (9–10)		Rocksalt-glucose	Cu–Rocksalt-glucose
	Pos1	–1250.6314779	–1381.1007491
	Pos2	–1250.6190392	–1381.122466
	Pos3	–1250.6133778	–1381.1328698

Cu cation, and the bond remains with the same values. So maybe this doped compound can be applied as a sensitive element to sensor technology. Also, it is observed that the symmetry group ( $C_1$ ) is conserved. For  $n = 3$ , the distance between Zn and O is not symmetrical enough like that of the non-doped cluster. Also, the total energy is equal to –553.03 a.u. The  $(ZnO)_4$  cluster shows that the Zn–O contact varies from 1.83 to 1.79 Å, symmetrically. The Zn–O–Zn angle is equal to 153°. It is observed that the angle Zn–O–Cu is around 144°. The doping almost does not modify the structural organization of the compound. The symmetry group (Cs) has been preserved. The total energy of this system is –693.91 a.u. From Figure 3b, for the wurtzite cluster, the relaxation energy is around –693.86 a.u. The breaking bond between the cation and the nearby atoms proves that a charge transfer phenomenon takes place during the doping. The same interpretation is found for the rocksalt cluster. It is concluded that the doping improves the structural stability of the studied clusters. The breakage of the bonds after doping indicates that the valence electrons of the Cu cation exert rather strong forces on the close atoms, which proves that all the electrons are torn off by the metal. This phenomenon will be explained in detail in the next section. So, the doped clusters are very suitable for sensor applications.

#### 4.2. Raman analysis

Figure 4(a–d) show the calculated and the experimental Raman spectra of the  $(ZnO)_4$  clusters. It is detected in a high absorption band at 763 (Cu-ring), 653 (Cu-wurtzite), and 443  $cm^{-1}$  (Cu-rocksalt), respectively. These strong absorptions for stretching modes are assigned to the vibration of the ZnO groups. The experimental signal is located around 751  $cm^{-1}$ . The experimental value is much closer to that of the Cu ring shape than that of other systems. This result proves that the compound experimentally formed is one with a ring shape and not wurtzite or rocksalt. This idea is well confirmed by the energetic interpretation section. In addition, absorption bands of medium intensity were obtained in the three clusters, which are equal to 475, 459, and 485  $cm^{-1}$ , respectively. The experimental value is approximately 481  $cm^{-1}$ . It is concluded that the Cu-ring and Cu-rocksalt values are close to the experimental one. A breaking of the Cu–O group is found (see Figure 4), so, it was concluded that the phonon of the Cu atom forced the shift of this frequency in the wurtzite shape. Additionally, the Raman spectra

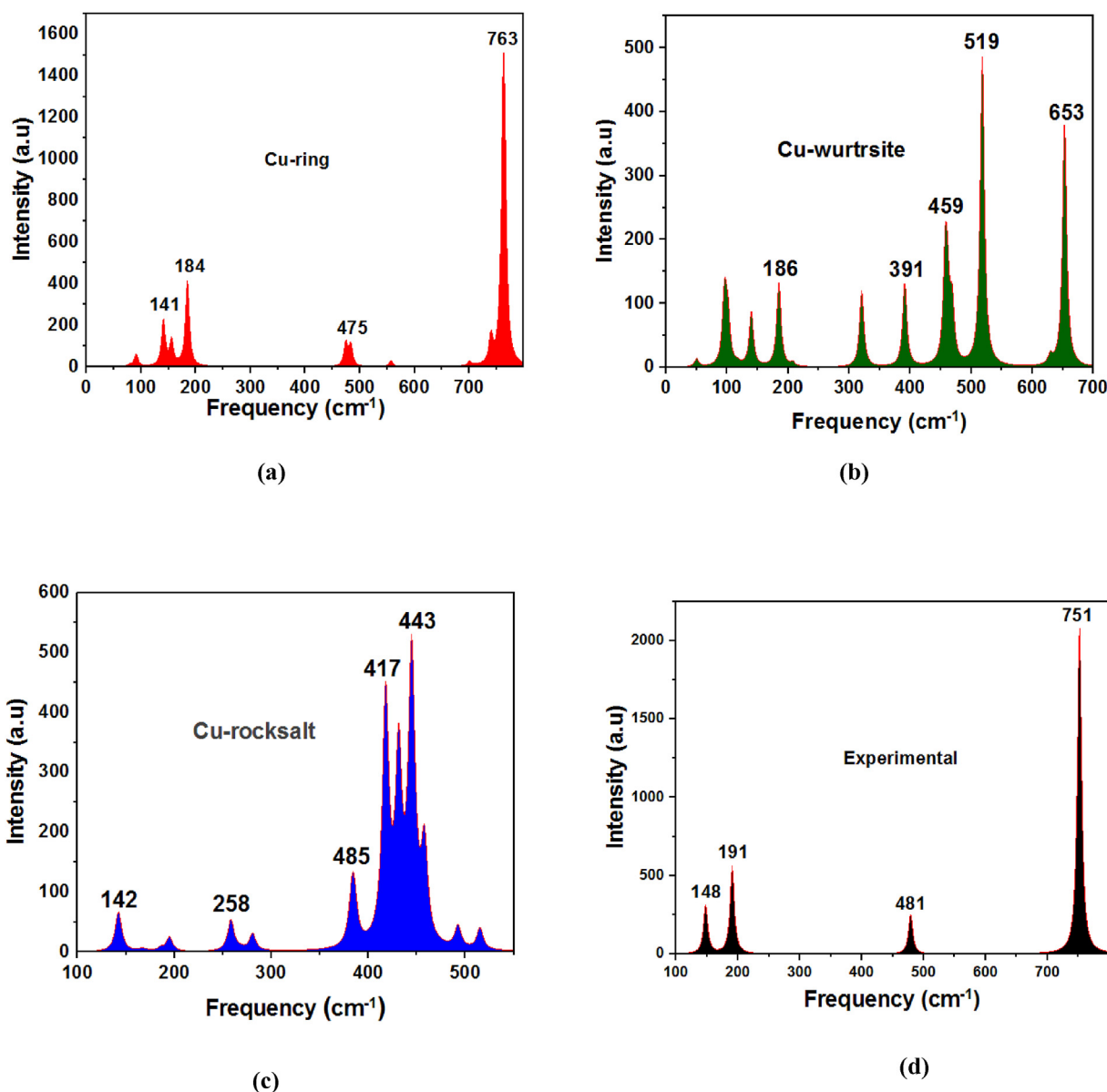
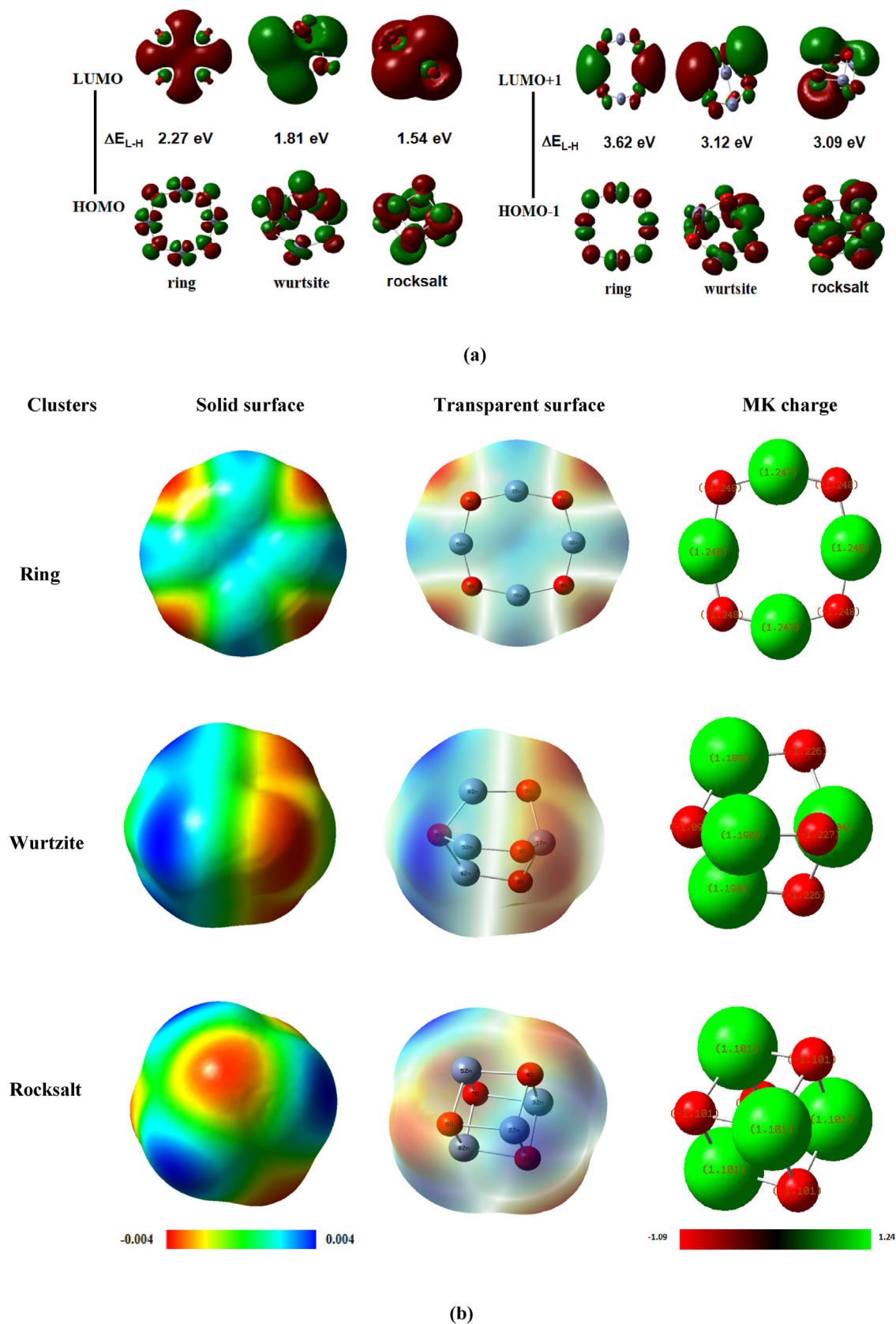


Figure 4. Theoretical Raman spectra of Cu-ring (a), Cu-wurtzite (b), and Cu-rocksalt (c) and the experimental spectrum of Cu-(ZnO)<sub>4</sub> cluster.

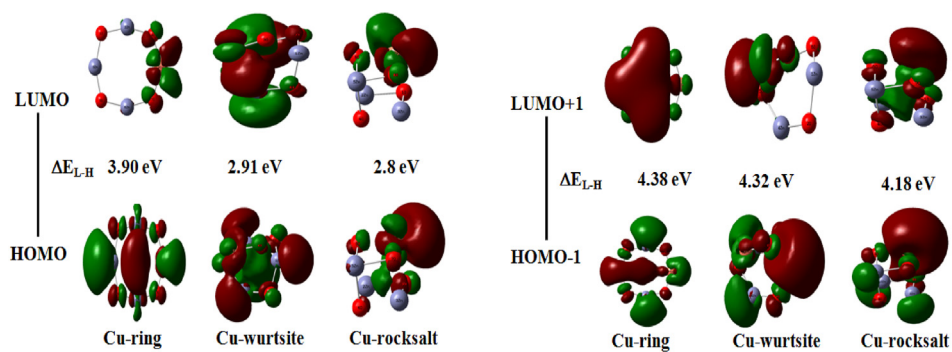
show frequency bands located at 184 (Cu-ring), 186 (Cu-wurtzite), and (189) cm<sup>-1</sup>, respectively. It is obtained a small shift beyond 0.3 cm<sup>-1</sup>. Herein, the experimental value is equal to 191 cm<sup>-1</sup>. Therefore, there is a good agreement between all the DFT values for all systems with the experimental measurements. The strain vibration out of the plane of the O atom is also assigned. It shows a low intensity frequency located at 141, 139, and 142 cm<sup>-1</sup> for all compounds, respectively, while the experimental value is about 148 cm<sup>-1</sup>. The Cu atom retains the frequency bands. So, there is a good agreement between the DFT results and the experimental ones. In the Cu-wurtzite, the theoretical frequency is located between 300 and 400 cm<sup>-1</sup>. These absorption peaks correspond to the elongation vibration of the O atom connected to the Cu metal. It is shown that these two peaks are absent in the experimental spectrum. It clearly shows an absorption band with medium intensity in the Cu-rocksalt shape at 258 cm<sup>-1</sup>. This low frequency corresponds to the -Zn-O-Zn and -O-Cu-O- coupled modes. This frequency is not observed in the experimental Raman spectrum.

#### 4.3. HOMO-LUMO and MEP-MK iso-surface

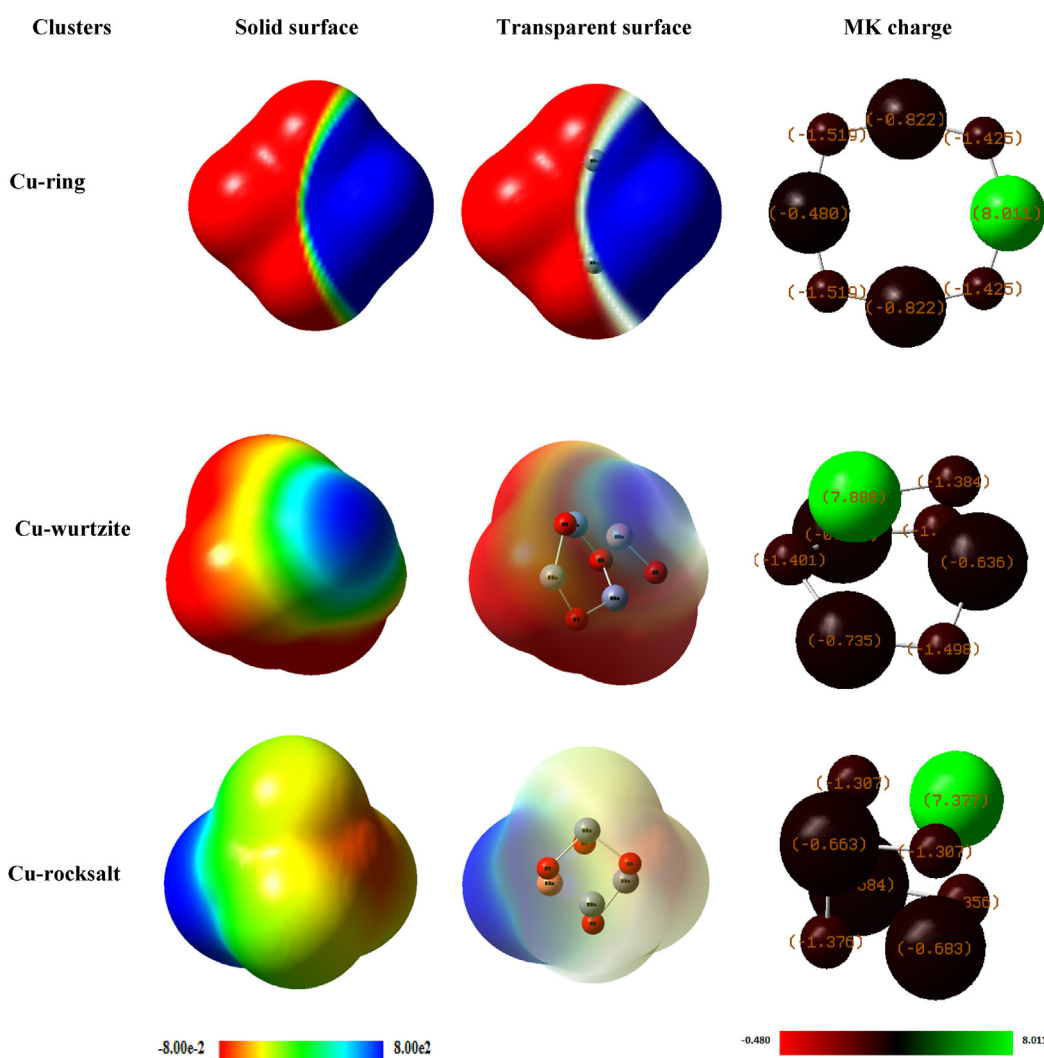
The Highest Occupied Molecular Orbital (HOMO) and the Lowest Unoccupied Molecular Orbital (LUMO) iso-surfaces characterize the electronic absorption from the ground state to an excited state in the studied compounds. The localization of the molecular orbitals gives quite clear information on the chemical reactivity of the clusters and indicates the characteristics of the donor-acceptor groups, which favor the existence of inter- or intra-molecular charge transfer phenomena in such materials (Figures 5 and 6). The location of molecular orbitals has been discussed before and after doping to understand the effect of Cu-doping on the charge transfer phenomenon and on the chemical reactivity of the clusters. To better understand, the distributions of the electronic charges before and after doping, the molecular electrostatic potential (MEP) analysis and Mulliken charges of all stable (ZnO)<sub>4</sub>, and Cu-Zn<sub>3</sub>O<sub>4</sub> systems are interpreted (see Figures 5 and 6). The electron density of the HOMO orbital is localized on all the atoms (O and Zn) forming the ring of the



**Figure 5.** (a): Frontier molecular orbital, (b): MEP analyses, and Mulliken charge population of  $(ZnO)_4$  (Ring, wurtzite, and rocksalt shape) calculated at the B3LYP-D3/Lan12DZ level of theory.



(a)



(b)

**Figure 6.** (a): Frontier molecular orbitals, and (b): MEP surfaces, and Mulliken charge populations of the Cu-Zn<sub>3</sub>O<sub>4</sub> clusters (Cu-Ring, Cu-wurtzite, and Cu-rocksalt shapes) calculated at the B3LYP-D3/Lanl2DZ level of theory.

(ZnO)<sub>4</sub>. The valence electrons are excited toward the LUMO with energy of 2.27 eV. The LUMO orbital for the ring shape shows that the electron concentrations are localized practically on the entire cavity surface. This compound easily forms a donor-acceptor cross with a guest. The (ZnO)<sub>4</sub> is suitable for use as a sensible sensor element. From Figure 5(a), it is observed that the orbital HOMO-1 with the ring shape is localized surrounding the O and Zn atoms, almost having the same form as the HOMO iso-surface. Concerning the LUMO+1, the electrons are split symmetrically on the surface level of the cavity. The  $\Delta E_{L-H}$  energy value is equal to 3.62 eV. For the wurtzite shape, the valence electrons (HOMO) are mostly localized on the Zn–O groups, after excitation, these electrons cross a forbidden band of energy equal to 1.81 eV to be localized on the above Zn–O group. This idea explains that the localized electronic concentration surrounding the Zn–O group can be strongly linked to an acceptor element located in front of this group. Therefore, the wurtzite cluster can be a good sensor of chemical entities. The HOMO-1/LUMO+1 energy is equal to 3.12 eV. According to the proportionality between the wavelength (nm) and the energy in eV of  $\lambda$  (nm) = 1240/E(eV), the Zn–O ring presents a wavelength of 546 nm, and the wurtzite form has a wavelength equal to 343 nm. The ring shape absorbs in the blue ray while the wurtzite absorbs an excitation wavelength in the ultra-violet region. From Figure 5, the rocksalt shape shows that the electrons located around of all the O and Zn atoms (HOMO plot) are migrated to the excited state (LUMO plot), which is located around the entire rocksalt cluster. This system clearly appears as a reddish ball, so it is practically an acceptor system. So, this compound can be very useful in chemical sensor applications. The gap energy is equal to 1.54 eV. From this energy, the wavelength is roughly 800 nm. So, the rocksalt form is capable of absorbing the red rays. According to the relationship between the conductivity parameter and the gap energy ( $\sigma \propto \exp(E_g/k_B T)$ ), it is indicated that the ring shape of (ZnO)<sub>4</sub> has a  $\sigma$  equal to 9.67 eV. The wurtzite cluster presents a conductivity around 6.11 eV, and the rocksalt shape has the lowest conductivity (4.66 eV). It is concluded that the (ZnO)<sub>4</sub> is the most conductive material. In Figure 5(b), from 3D-MEP, it is clearly obtained that the acceptor sites (red spots) are located surrounding the O atoms or the electron donor sites (blue spots) are located around the Zn atoms. The charge atomic populations given by the Mulliken charges show that the ring, wurtzite, and rocksalt clusters are characterized by O atomic charges of –1.24, –1.22, and –1.10 a.u., respectively. Moreover, this result confirmed that these clusters could form a couple of donor-acceptor electrons with the guest.

From Figure 6(a), it is observed that the HOMO orbital of the Cu-ring cluster is mainly located on the O and Zn atoms. The valence electrons are absorbed with energy of 3.90 eV to make the transition towards the LUMO band. The  $\lambda$  of the Cu-ring is equal to 317.94 eV. In comparison between the ring shape before and after doping, there is a shift from the blue light to the ultra-violet region of 228.31 nm. So, it is concluded that the Cu doping totally modifies the chemical behavior of these materials. It is shown that the distribution of the LUMO is mainly located surrounding the Cu cation. From the solid and transparent MEP iso-surfaces depicted in Figure 6(b), it is shown that the Cu-ring has the electrophilic sites (electron acceptors/red spot) located in the non-doped region, and, the nucleophilic sites (electron donors/blue spot) are located surrounding to Cu atom. From the MK charges, it can be observed that the charges of the Zn atoms are positive and those of the O atoms are negative before doping, but are totally modified to negative after doping. The values of the charges of Zn and O atoms vary from –0.822 |e| to –1.51 |e|, respectively. These results concluded that the ring shape of (ZnO)<sub>4</sub> is a suitable system for sensor applications. The HOMO-1 plot appears to be located on the Cu atom and the two symmetrical O atoms. The LUMO+1 orbital is mainly located in the center of the ring. The HOMO-LUMO energy is equal to 4.38 eV. Concerning the Cu-wurtzite, it is found that the HOMO isosurface is located around the Cu atom and the ZnO group. The gap energy is about 2.91 eV. From, Figure 6(a), it is indicated that the LUMO plot is mainly located surrounding the Cu cation. The HOMO–LUMO energy is equal to 2.91 eV. In comparison between the two

systems, before and after doping, it is concluded that there is a shift in the gap energy of 1.10 eV. So, the doping Cu enriches the chemical reactivity of the material, making it harder and more stable. The  $\lambda$  of the Cu-wurtzite is 426 eV. It has been concluded that this compound absorbs blue rays. As shown in MEP, it can be seen that the attraction sites (red color) coexist around the cyclic base. The repulsive sites are located on the CuO group. The MK population charges show that the Cu atom charge is about 8.01 |e|. The charge of Zn and O atoms appears to vary from –0.63 to –1.49 |e|. Again, the Mulliken charges demonstrated that after doping, the system will be more reactive. These findings concluded that Cu-wurtzite is very suitable for use as a sensible element in sensors. In addition, it is shown that the HOMO-1 and LUMO+1 orbitals are located around the Cu atom. The gap energy is equal to 4.32 eV. Finally, the same interpretation is found for the Cu-rocksalt system. The HOMO-LUMO energy of this cluster is about 4.18 eV. The  $\lambda_{\text{Cu-rocksalt}}$  is equal to 442 nm. After Cu-doping, it has a blue shift of 363 nm. The Cu-rocksalt becomes harder, more polar, and more reactive than before the doping. It is concluded that the Cu-ring is more conductive than the Cu-wurtzite, and Cu-rocksalt.

A deep discussion of the frontier molecular orbital, MEP-MK analysis, and conductivity parameters demonstrated that the doping clusters are more sensitive to interacting with the glucose.

#### 4.4. Glucose sensing with the optimized Cu-Zn<sub>n-1</sub>O<sub>n</sub> clusters

All the possible conformations of the Zn<sub>n</sub>O<sub>n</sub> and the Cu-Zn<sub>n-1</sub>O<sub>n</sub> (n = 2–4) clusters before complexation with glucose were optimized (see Figure 7 (a) and (b)). These stable conformations are applied for glucose detection (see Figure 8). The optimized geometry of the glucose entity is depicted in Figure 7 c).

In the complex formation of the (ZnO)<sub>n</sub> metal oxides with glucose, it is observed that the (ZnO)<sub>n</sub> crown ring structure converts to a practically planar or hooked structure [52]. On the other hand, in the formation of the stable Cu-Zn<sub>n-1</sub>O<sub>n</sub> complexes, it is observed that the clusters are coordinated with the electrophilic Cu atom, which is more active and has a d<sup>9</sup> configuration, compared to the Zn atom with a d<sup>10</sup> configuration. It is observed that the Zn atom is more electropositive, and therefore the Cu atom is attracted towards the glucose ring. In Cu-Wurtzite-glucose and Cu-Rocksalt-glucose complexes, the glucose is coordinated over the copper atom, and the cubic structure is turned into a basket-like structure, and the missing edges are bonded with coordinated covalent bonds between metal and O atoms, and hydrogen bonds (C–O···H···O) [53]. In the complex formation, the unpaired 2p electrons of the O atoms are attracted by the positively charged Zn and/or Cu atoms [53]. For the classical hydrogen bonding, the angle between them is between 135° and 225° and the distance D···A is around 2.5 Å [54]. Figure 9 shows that the structure of complexes has hydrogen bonds between OH groups and adjacent O atoms. The analysis of the H-bonds is given in Table 3. Two H-bonds are formed in the Zn<sub>3</sub>O<sub>3</sub>-glucose and the Zn<sub>4</sub>O<sub>4</sub>-glucose complexes, and one H-bond is observed in the Cu–ZnO<sub>2</sub>-glucose and Cu–Zn<sub>2</sub>O<sub>3</sub>-glucose complexes. Due to the radius of the Cu atom being larger than that of the Zn atom and therefore having a larger steric effect, the O atoms in the metal oxide cannot get close enough to the glucose unit to form one H-bond through OH group. An energy diagram that summarizes the order of stabilities of the Cu-Zn<sub>n-1</sub>O<sub>n</sub>-glucose complexes has been shown in Figure 10.

##### 4.4.1. FT-IR analysis

The IR spectra of complexes are given in Figure 11(a–e) in the range of 4000–0 cm<sup>–1</sup>. The peaks in the range of 3750–3626 cm<sup>–1</sup> and 3840 cm<sup>–1</sup> (weak) are attributed to O–H stretching modes in the glucose ring of the Zn<sub>2</sub>O<sub>2</sub>-glucose complex, while this peak (Zn–O–H) drastically decreases to 3367 cm<sup>–1</sup> (strong) in the Cu–ZnO<sub>2</sub>-glucose complex due to the hydrogen bonding with the carbonyl group (Zn–O–H···O=C–H) (Figure 9) [55, 56]. In the IR spectra of the complexes, the observation of non-hydrogen bonding OH stretching peaks at higher frequencies and

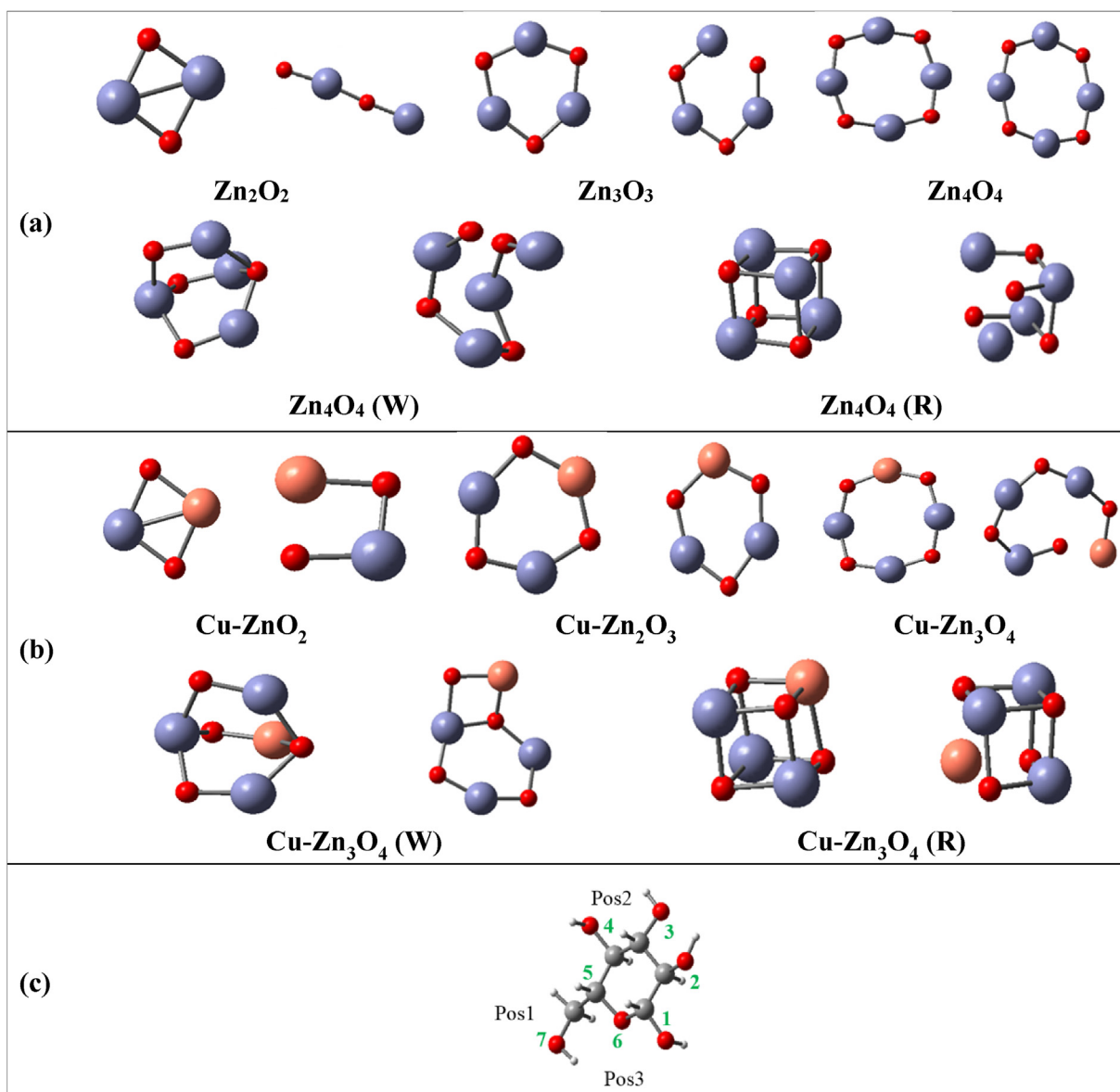


**Figure 7.** (a)  $Zn_nO_n$  and (b)  $Cu-Zn_{n-1}O_n$  structures, obtained from crystal information (left side), and the corresponding optimized structures (right side) for  $n = 2-4$  calculated at the B3LYP-D3/LanL2DZ level of theory. Wurtzite (W) and Rocksalt (R) structures are isomers of  $Zn_4O_4$ . (c): glucose entity.

hydrogen bonding OH stretching peaks at lower frequencies is also consistent with the literature [55, 56]. Unlike the  $Zn_2O_2$ -glucose complex, the peak, which was detected at  $1647\text{ cm}^{-1}$ , is attributed to the stretching vibration of the carbonyl group in the  $Cu-ZnO_2$ -glucose complex [55]. In Figure 8, it is observed that the Cu atom forms a stable complex in square plane geometry with four O atoms, two of which are in the glucose ring and the other two come from the  $CuZnO_2$  cluster [56, 57]. Aliphatic C-H symmetrical and asymmetric stretching vibrations in  $Zn_2O_2$ -glucose complex were detected as weak peaks at  $3116-2977\text{ cm}^{-1}$  [58], while these weak peaks widen up and down field and shift to  $3147-2924\text{ cm}^{-1}$  in  $Cu-ZnO_2$ -glucose complex. The C-O stretching signals shifted to the lower frequencies and weakened in the  $Cu-ZnO_2$ -glucose complex due to the coordination of the O atoms of the glucose ring (O1, O7) and the  $Cu-ZnO_2$  cluster with the Cu atom in the square planar geometry [58]. The peaks observed between  $600-500\text{ cm}^{-1}$  are attributed to Zn(II)-O and Cu(II)-O stretching modes, according to the literature [59, 60]. O-H, C-H, C-O, Zn-O and Cu-O stretching peaks were detected in similar regions in all complexes, as seen in Table 4. The IR spectrum of the  $Cu-Zn_2O_3$ -glucose complex (4) (Figure 11(b)) showed

strong peaks at  $2604\text{ cm}^{-1}$ , which are observed in the theoretical spectrum, are caused by hydrogen bond formation ( $C-O\cdots H\cdots O-Zn$ ) (see Figure 9) and Fermi resonance [56]. The presence of O-H bending signals, detected as medium peaks at  $1232\text{ cm}^{-1}$ ,  $937\text{ cm}^{-1}$  and  $875\text{ cm}^{-1}$  [61], respectively, in the  $Zn_3O_3$ -glucose complex, confirms the coordination of the Zn atom and glucose O atom. Due to the lack of coordination in the  $Cu-Zn_2O_3$ -glucose complex, the Cu-O stretching vibrational modes were detected at  $702\text{ cm}^{-1}$ ,  $601\text{ cm}^{-1}$  and  $454\text{ cm}^{-1}$  (Figure 11(b)), respectively, at higher frequencies than for the  $Cu-ZnO_2$ -glucose complex [56, 59]. Similar to IR spectrum of the  $Cu-Zn_2O_3$ -glucose complex (4), the IR spectrum of the  $Zn_4O_4$ -glucose complex (5) (Figure 11(c)) presents strong peaks at  $2928\text{ cm}^{-1}$  and  $2258\text{ cm}^{-1}$  due to the hydrogen bond formation ( $C-O\cdots H\cdots O-Zn$ ) and Fermi resonance [56]. For  $Cu-Zn_3O_4$ -Glu complex (6), it is observed that the Cu-O stretching peak, located between  $763$  and  $549\text{ cm}^{-1}$ , shifts to higher frequencies, compared to complexes  $Cu-Zn_2O_3$ -Glu (4) and  $Cu-ZnO_2$ -Glu (2) [59]. The IR spectrum of the Wurtzite-glucose (7) complex (Figure 11(d)), As expected, the two Zn-O-H stretching signals were observed, formed as result of the complexation and located in the ( $Zn_4O_4$ ) cluster structure; they were

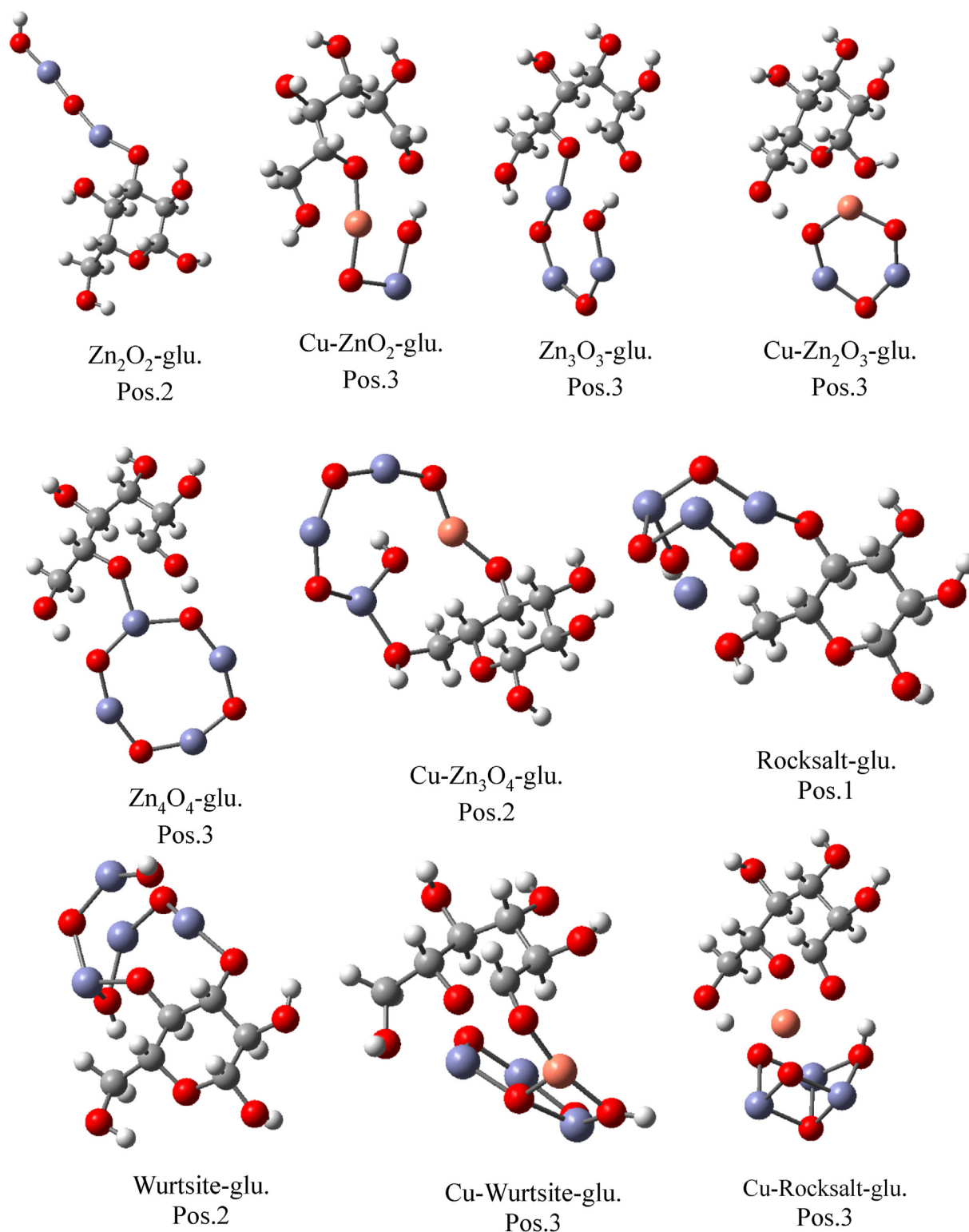


**Figure 8.**  $(ZnO)_n$ -glucose and  $Cu-Zn_{n-1}O_n$ -glucose optimized structures for  $n = 2-4$  were calculated at the B3LYP-D3/LanL2DZ level of theory. Wurtzite (W) and Rocksalt (R) structures are isomers of  $Zn_4O_4$ .

detected between  $3861 - 3604 \text{ cm}^{-1}$ , respectively [55, 59]. The signals observed at  $3861 \text{ cm}^{-1}$  belong to the non-hydrogen bonding OH groups, and another peak observed at  $3604 \text{ cm}^{-1}$  belongs to H-bonded [55]. Compared to Wurtzite-glucose with the effect of the Cu atom, Zn–O stretching peaks in Cu-Wurtzite-glucose (8) were detected at higher frequencies [55, 59]. In the structure of the Rocksalt-glucose complex (9), it is seen that the cubic structure of the metal oxides ( $Zn_4O_4$ ) turns

into an s-shaped structure [62]. However, in the Cu-Rocksalt-glucose complex (10), it is observed that the  $Cu-Zn_3O_4$  metal oxide cubic structure is not completely destroyed, but the O atom ( $Zn_2O-H$ ) in the cubic structure forms three bonds. Due to the weakening of the bond between this positively charged O atom and H, the  $Zn_2O-H$  stretching vibrational mode shifted to lower frequencies and was detected at  $3643 \text{ cm}^{-1}$ . The Cu atom is not bonded in the stable structure of

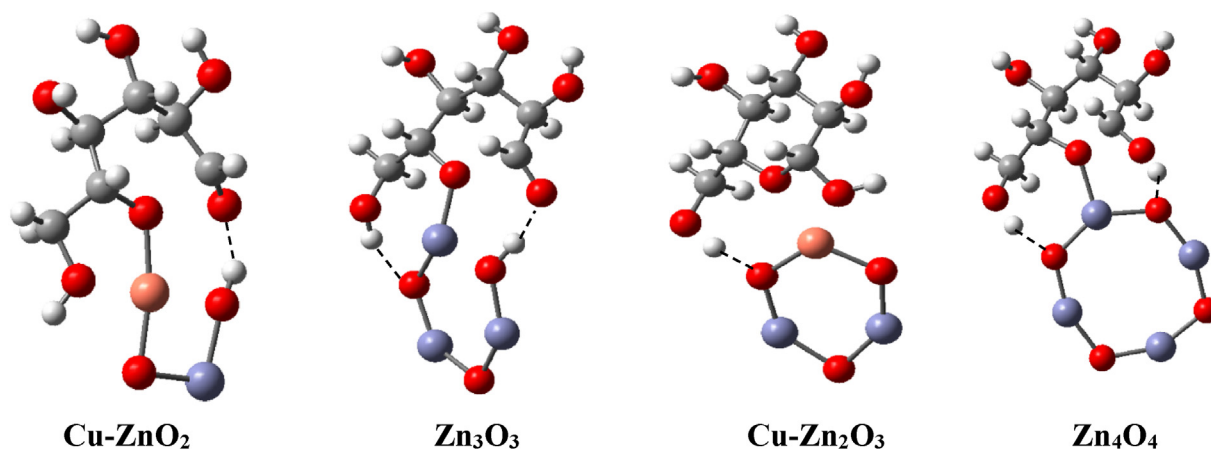


Figure 9. H-bonding interactions form between the stable clusters and the glucose.

Table 3. Hydrogen-bonding analysis of the relevant complexes ( $\text{\AA}$ ,  $^\circ$ ).

Complexes	D-H...A	D-H	H...A	D...A	D-H...A
Cu-ZnO <sub>2</sub> -Glu-Pos3 (2)	O-H...O	0,99	1,73	2,65	152
Zn <sub>3</sub> O <sub>3</sub> -Glu-Pos3 (3)	O-H...O	1,01	1,73	2,55	135
	O-H...O	1,01	1,63	2,58	153
Cu-Zn <sub>2</sub> O <sub>3</sub> -Glu-Pos3 (4)	O-H...O	1,04	1,49	2,52	170
Zn <sub>4</sub> O <sub>4</sub> -Glu-Pos3 (5)	O-H...O	1,02	1,60	2,59	161
	O-H...O	1,06	1,47	2,46	153

Cu-Rocksalt-glucose complexes (see Figure 11(e)). Since the Cu atom in the bulky cubic structure cannot fully approach the glucose ring in the pos3 region due to its steric effect, coordinated covalent bond formation

occurs between the Cu and O atoms instead of the covalent bonds in the formation of the stable complexes. In other compounds (8, 6, 4, and 2) with the effect of Cu atom, the Zn-O bond shifted to higher frequencies when it was compared with non-copper complexes (7, 5, 3, and 1), respectively. Table 4 summarizes the calculated vibrational frequencies of the complexes.

#### 4.4.2. HOMO-LUMO iso-surface

HOMO and LUMO analyses were performed to examine the electronic properties of the compounds [63, 64]. The HOMO-LUMO gap energies, ionization potential, electron affinity, and the global reactivity parameters, such as electronegativity, chemical hardness, chemical softness, chemical potential, and electrophilic index, are given in Table 5 and calculated from the HOMO and LUMO energies.

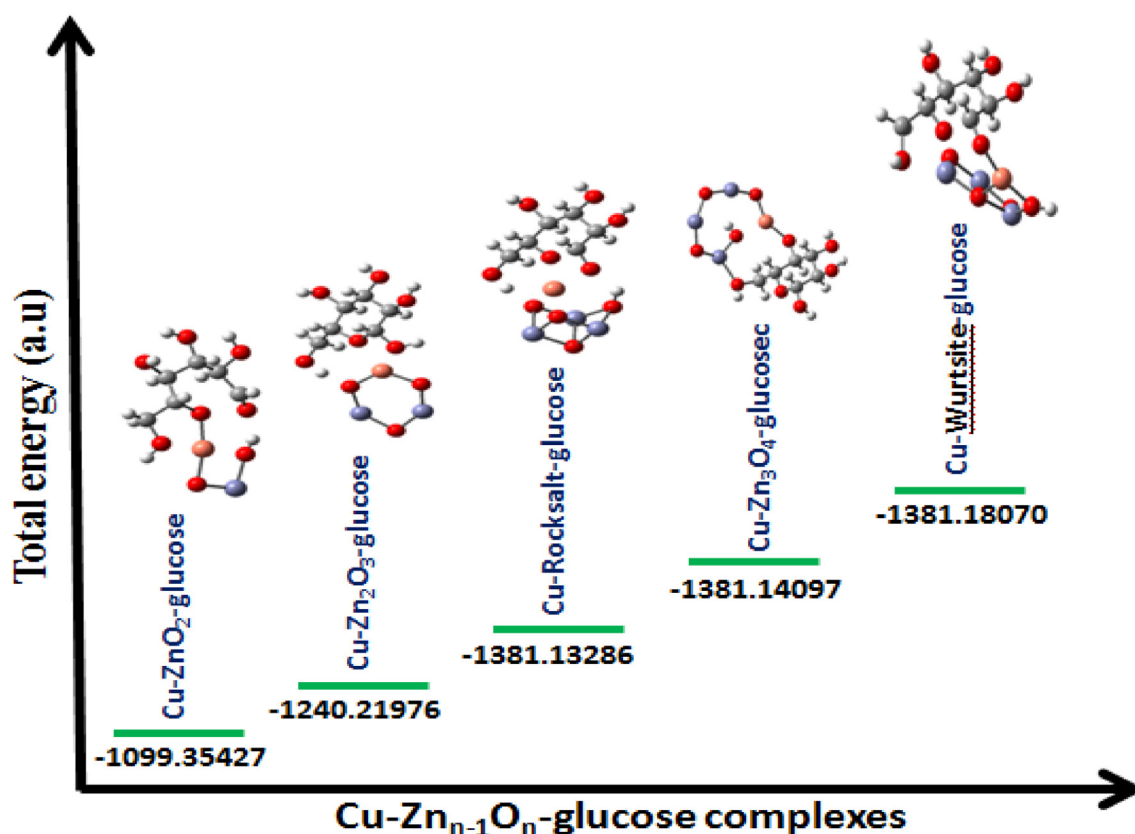


Figure 10. The total energy representation for the Cu-Zn<sub>n-1</sub>O<sub>n</sub>-glucose complexes.

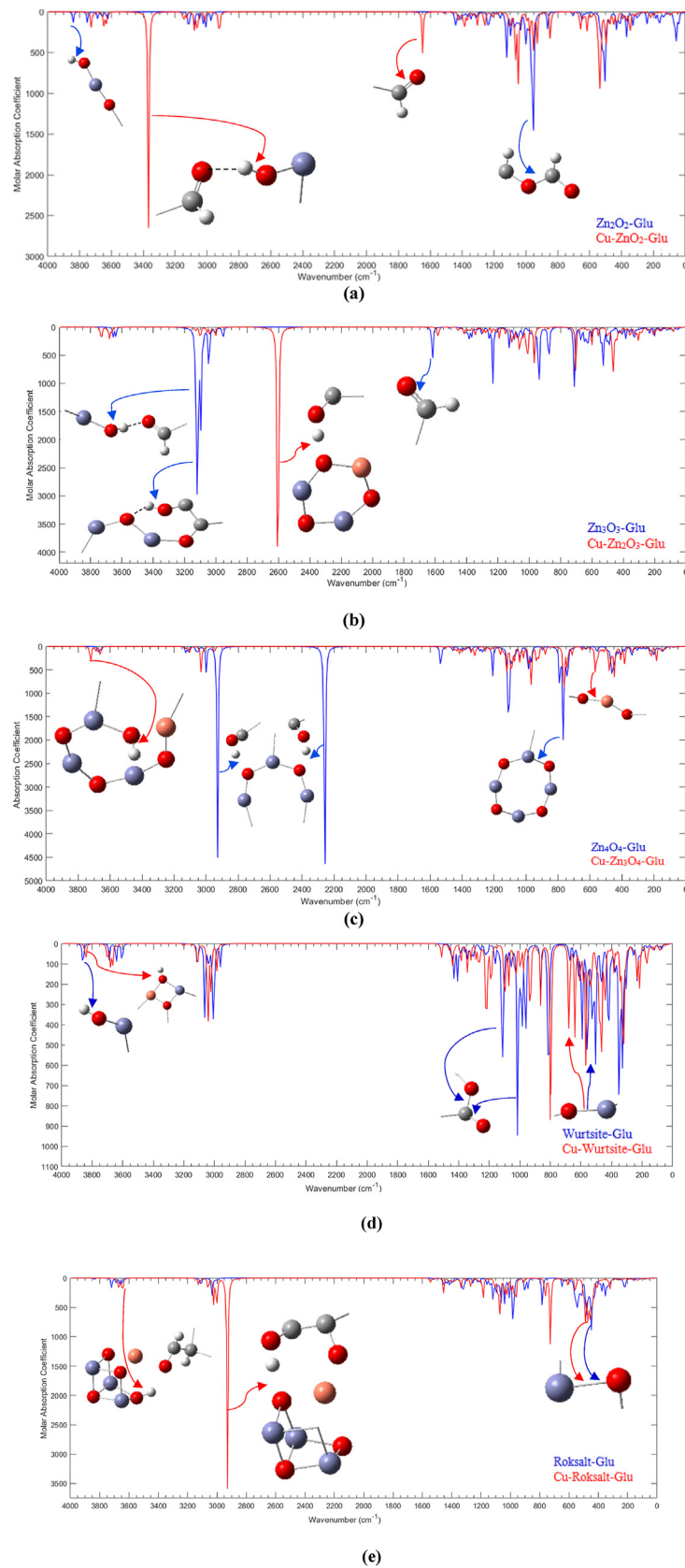


Figure 11. (a–e): IR spectra of the (ZnO)*n*-glucose and Cu-Zn-1-On-glucose complexes calculated at the B3LYP-D3/LanL2DZ level in the gas phase.

**Table 4.** Vibrational frequencies ( $\text{cm}^{-1}$ ) of the complexes at B3LYP-D3/LanL2DZ level of theory.

Complex	$\nu_{\text{O-H}}$	$\nu_{\text{C-H}}$	$\nu_{\text{C=O}}$	$\nu_{\text{C-O}}$	$\nu_{\text{Zn-O}}$	$\nu_{\text{Cu-O}}$
1 Zn <sub>2</sub> O <sub>2</sub> -Glu	3840 w 3750-3626 w	3116-2977 w	–	1120 m 955 s	522 m	–
2 Cu-ZnO <sub>2</sub> -Glu	3726-3634 w 3367 s	3147-2924 w	1647 m	1066 m 1047 m 951 w	588 w 547 m	658 w 615 w 474 w
3 Zn <sub>3</sub> O <sub>3</sub> -Glu	3659-3638 w 3131-3097 s	3046-2955 w	1618 m	1127 m 937 m	713 m 539 m 432 w	–
4 Cu-Zn <sub>2</sub> O <sub>3</sub> -Glu	3731-3663 w	3130-3001 w	–	1063 w 1011 m 967 m	702 s 601 m	702 m 601 w 454 m
5 Zn <sub>4</sub> O <sub>4</sub> -Glu	3676-3658 w	3128-2999 w	–	1107 s 1085 m 966 m	766 s 746 m 465 m	–
6 CuZn <sub>3</sub> O <sub>4</sub> -Glu	3728-3721 w 3689-3659 w	3219-2948 w	–	1121 w 1090 w 967 w	741 m 481m	763 m 549 m
7 Wurtsite-Glu	3861-3858 w 3688-3604 w	3109-2961 m	–	1117 m 1014 s 962 m	593 m 525 w 420 m	–
8 Cu-Wurtsite-Glu	3843 w 3700-3636 w	3201-2982 m	–	1220-932 m	677 m 638 m	532 m 475 m
9 Rocksalt-Glu	3835 w 3717-3646 w	3208-2995 w	–	1117-974 m	541 m 480 m 443 s	–
10 Cu-Rocksalt-Glu	3672-3659 w 3643 w	3127-2997 w	–	1186 w 1070 m 963 m	559 w 486-467 m	–

w: weak; m: medium; s: strong.

The magnitude of the difference between LUMO-HOMO ( $\Delta E$ ) indicates the electronic stability of the molecule. The complexes present the following chemical stability in the following order: Zn<sub>2</sub>O<sub>2</sub>-glucose > Zn<sub>4</sub>O<sub>4</sub>-Glu > Zn<sub>3</sub>O<sub>4</sub>-glucose > Rocksalt-glucose > Wurtzite-glucose. The high values of  $\Delta E$  and  $\eta$  for the Zn<sub>2</sub>O<sub>2</sub>-glucose complex point out that it is more stable and less polarizable than the others. The low electrophilicity index ( $\omega$ ) and low  $|\mu|$  values of Zn<sub>2</sub>O<sub>2</sub>-glucose complex compared to others infer good nucleophilic behavior. Conversely, the Wurtzite-glucose complex has the highest electrophilicity index ( $\omega$ ) which means good electrophile behavior.

In the iso-surfaces of the HOMO and LUMO (see Figures 12, 13, and 14 and S6–S7), it can be seen that the HOMO distribution consists

mainly of the metal oxide cluster, besides the glucose ring formed by the  $\pi$  electrons of the O atoms. On the other hand, it is seen that the LUMO distribution of the complexes consists mainly of the d electrons of the Cu(II) and Zn(II) atoms of the metal oxide clusters. The charge distribution in LUMO is concentrated on the d orbitals and mostly on the Zn atoms with the  $d^{10}$  full configuration. The blue color in the MEP maps (see Figure 15) indicates that the charge distribution in LUMO is mainly concentrated on the d orbitals and mostly on the Zn atoms with the  $d^{10}$  configuration. HOMO is mainly located around the O atoms of the complexes, whereas LUMO is located around the metal atoms. The electronegative O atoms are given a red color in MEP iso-surfaces, while the green color indicates a neutral region because of the

**Table 5.** HOMO-LUMO energies (eV) and the calculated global reactivity parameters of the most stable complexes calculated at the B3LYP-D3/LanL2DZ level of theory.

Compound	LUMO	HOMO	$\Delta E$ (eV)	IP (eV)	EA (eV)	X (eV)	H (eV)	S (eV) <sup>-1</sup>	M (eV)	$\Omega$ (eV)
Zn <sub>2</sub> O <sub>2</sub> -Glu (1)	-1,683	-6,932	5,249	6,932	1,683	4,308	2,625	0,190	-4,308	3,535
Cu-ZnO <sub>2</sub> -Glu (2)- $\alpha$	-3,392	-6,380	2,988	6,380	3,392	4,886	1,494	0,335	-4,886	7,989
Cu-ZnO <sub>2</sub> -Glu (2)- $\beta$	-3,372	-6,208	2,836	6,208	3,372	4,790	1,418	0,352	-4,790	8,090
Zn <sub>3</sub> O <sub>3</sub> -Glu (3)	-3,100	-6,821	3,721	6,821	3,100	4,961	1,860	0,269	-4,961	6,614
Cu-Zn <sub>2</sub> O <sub>3</sub> -Glu (4)- $\alpha$	-2,270	-6,312	4,042	6,312	2,270	4,291	2,021	0,247	-4,291	4,555
Cu-Zn <sub>2</sub> O <sub>3</sub> (4)- $\beta$	-2,973	-6,072	3,099	6,072	2,973	4,523	1,550	0,323	-4,523	6,599
Zn <sub>4</sub> O <sub>4</sub> -Glu (5)	-2,697	-6,898	4,201	6,898	2,697	4,798	2,100	0,238	-4,798	5,480
Cu-Zn <sub>3</sub> O <sub>4</sub> -Glu (6)- $\alpha$	-2,453	-6,510	4,057	6,510	2,453	4,482	2,029	0,246	-4,482	4,951
Cu-Zn <sub>3</sub> O <sub>4</sub> -Glu (6)- $\beta$	-3,692	-6,301	2,609	6,301	3,692	4,997	1,305	0,383	-4,997	9,569
Wurtsite-Glu (7)	-3,152	-6,240	3,088	6,240	3,152	4,696	1,544	0,324	-4,696	7,141
Cu-Wurtsite-Glu (8)- $\alpha$	-1,613	-5,973	4,360	5,973	1,613	3,793	2,180	0,229	-3,793	3,300
Cu-Wurtsite-Glu (8)- $\beta$	-3,552	-5,950	2,398	5,950	3,552	4,752	1,199	0,417	-4,752	9,415
Rocksalt-Glu (9)	-2,992	-6,273	3,281	6,273	2,992	4,632	1,641	0,305	-4,632	6,540
Cu-Rocksalt-Glu (10)- $\alpha$	-3,438	-6,539	3,101	6,539	3,438	4,988	1,550	0,322	-4,988	8,025
Cu-Rocksalt-Glu (10)- $\beta$	-3,426	-6,453	3,027	6,453	3,426	4,940	1,513	0,330	-4,940	8,062

Gap  $\Delta E$ : ( $E_{\text{LUMO}} - E_{\text{HOMO}}$ ), IP ( $-\text{HOMO}$ ): Ionization potential, EA ( $-\text{LUMO}$ ): Electron affinity, X ( $(\text{IP} + \text{EA})/2$ ): Electronegativity,  $\eta$  ( $(\text{IP} - \text{EA})/2$ ): Chemical hardness, S ( $1/2\eta$ ): chemical softness,  $\mu$  ( $-(\text{IP} + \text{EA})/2$ ): Chemical potential,  $\omega$  ( $\mu^2/2\eta$ ): Electrophilic index.

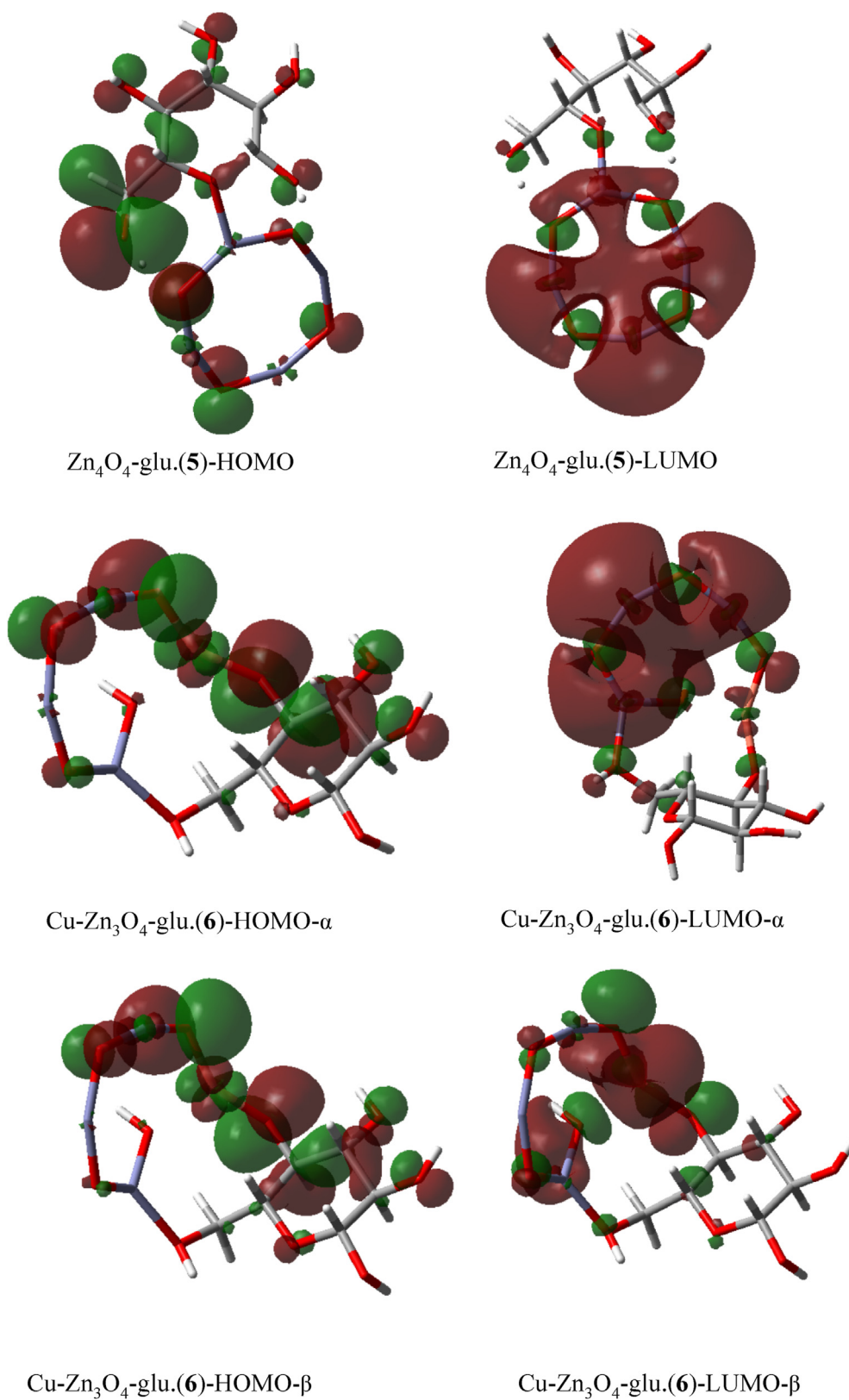


Figure 12. HOMO-LUMO plots of  $\text{Zn}_4\text{O}_4\text{-glu. (5)}$  and  $\text{Cu-Zn}_3\text{O}_4\text{-glu. (6)}$  Complexes.

electron transfer from O atoms towards the vacant d orbitals of the Cu atom in the complexation of Cu and glucose (Compounds **2**, **4**, **6**, **8** and **10**). As seen in Table 5, the energy difference between the HOMO and LUMO orbitals of the compound **2** is smaller than that of the compound **1**, which facilitates the electronic transition between orbitals

and increases the reactivity of the compounds. This is thought to be due to the electrophilic behavior of the Cu atom. Similarly, the electrophilic index in beta compounds (**2**, **4**, **6**, **8**, **10**) containing Cu atoms increases compared to the complexes containing only Zn atoms (**1**, **3**, **5**, **7**, **9**).

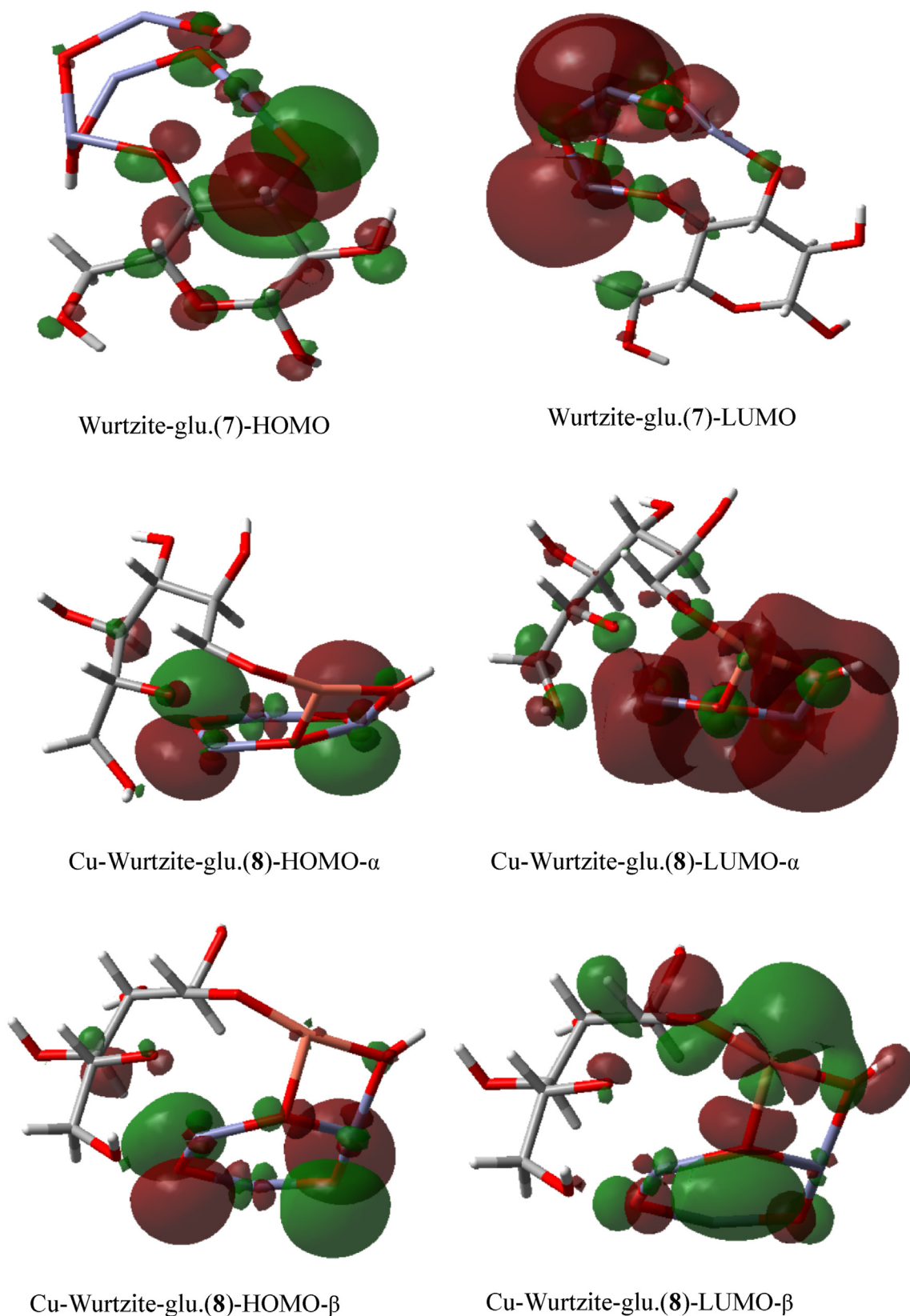


Figure 13. HOMO-LUMO plots of Wurtzite-glu. (7) and Cu-Wurtzite-glu. (8) Complexes.

#### 4.4.3. Glucose detection with electrochemistry

The cyclic voltammetry (CV) responses of ZnO and Cu-ZO in the 0.1 M NaOH in function to the glucose concentrations are presented in Figure 16(a-b). It is obtained a slight increase in ZnO current as a

function of glucose concentrations. This increase indicates the onset of oxidation peak currents. This idea indicated an excellent electrochemical detection linked to the catalytic effect of the electro-oxidation process of the CuOOH/Cu(OH)<sub>2</sub> couple of glucose into gluconolactone. In addition,

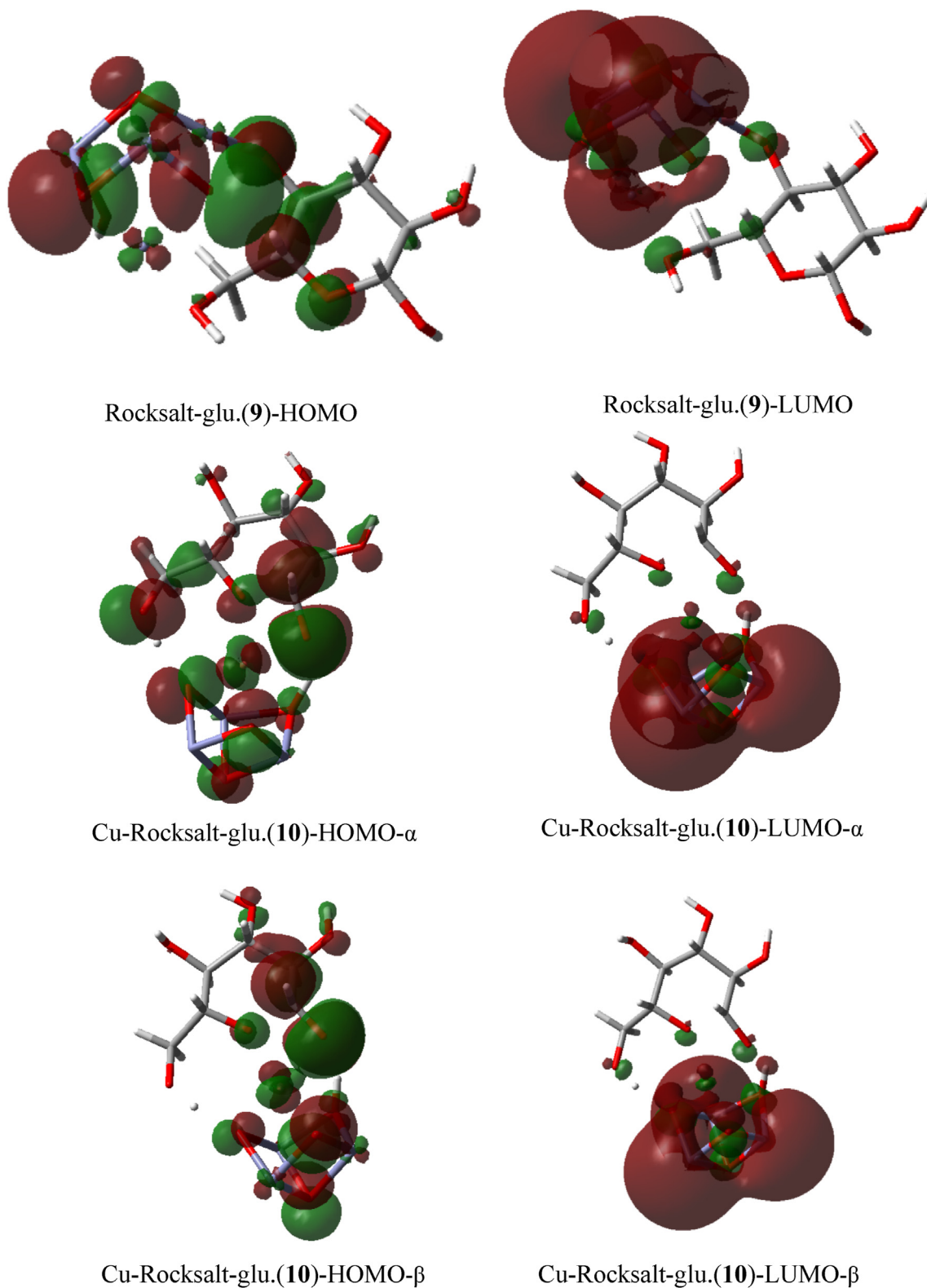
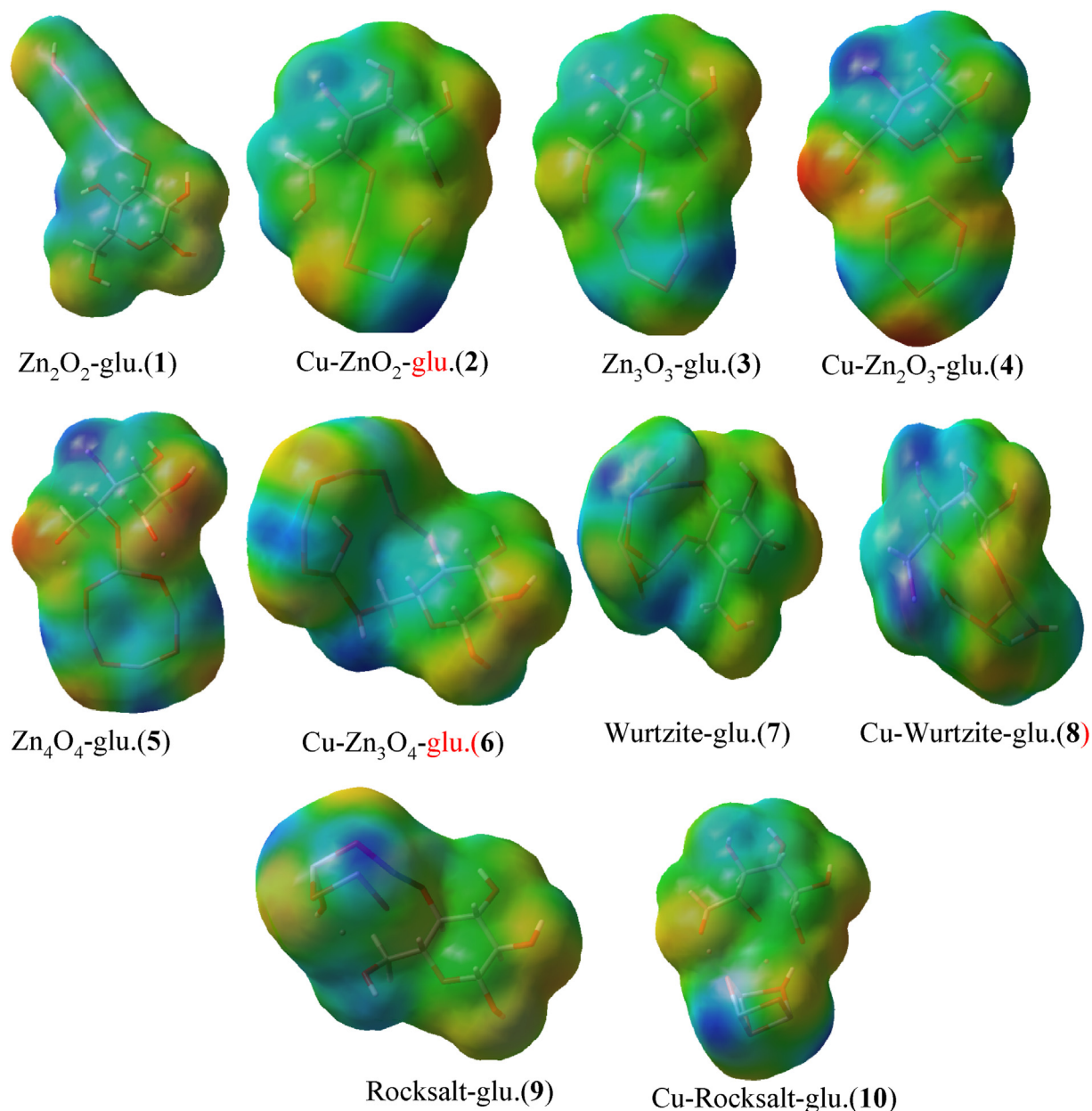


Figure 14. HOMO-LUMO plots of the Rocksalt-glu. (9) and Cu-Rocksalt-glu. (10) Complexes.

it is found that the copper doping plays an important role in glucose oxidation. This result proves that the addition of Cu provided high surface energy and increased surface area. It is concluded that the copper forces the existence of a large number of active sites, which facilitate the catalytic oxidation of glucose and provide a high enough conductivity to improve the transfer of electrons. From Figure 16(c), The ZnO exhibited a

linear region from 0.001 to 1  $\mu\text{M}$  with an equation of  $\Delta I/I_0 = (0.11) \times [\text{Glu}] (\mu\text{M}) + (0.12)$  ( $R^2 = 0.93$ ), where the slope is 0.11 of the response of sensors. According to the formula  $\text{LOD} = (3 \text{ standard deviations})/\text{slope}$ , the limit of detection of the optical sensor, was found to be  $9.5 \times 10^{-4} \mu\text{M}$ . Concerning the Cu-ZnO plot, a linear region is obtained from 0.001 to 1  $\mu\text{M}$ , with an equation of  $\Delta I/I_0 = (0.25) \times [\text{Glu}] (\mu\text{M}) + (0.1)$



**Figure 15.** MEPs diagrams of the  $(\text{ZnO})_n\text{-glucose}$  and  $\text{Cu-Zn}_{n-1}\text{O}_n\text{-glucose}$  complexes calculated at the B3LYP-D3/LanL2DZ level of theory for  $n = 2-4$ .

( $R^2 = 0.92$ ), where the slope is 0.25 of the response of sensors. It is noted that the LOD was found to be  $8 \times 10^{-4} \mu\text{M}$ . In healthy people, blood glucose concentration is  $0.8\text{--}1.2 \text{ mg/cm}^3$  ( $8.0\text{--}1.2 \times 10^{-7} \text{ g/L}$ ) as a standard, while this value can be maximum  $1.7 \text{ mg/cm}^3$  ( $1.7 \times 10^{-6} \text{ g/L}$ ) and minimum  $0.7 \text{ mg/cm}^3$  ( $7 \times 10^{-7} \text{ g/L}$ ) [65]. LOD values in the literature were determined as  $0.084\text{--}300 \mu\text{M}$  ( $8.4 \times 10^{-8}\text{--}3 \times 10^{-4} \text{ M}$ ) for glucose sensors [66]. From these data, we found that the  $\text{Cu-Zn}_{n-1}\text{O}_n$  is a good candidate for glucose detection.

#### 4.4.4. QTAIM analysis

The nature and type of interaction among  $(\text{Zn}_n\text{O}_n)$ ,  $\text{Cu-Zn}_{n-1}\text{O}_n$  and glucose is characterized and interpreted via the topological (QTAIM) and NCI-RDG analyses [67, 68]. The Bader's theory is the most prevalent technique for understanding the adsorption and the bonding interaction sites between guests and host species. This powerful approach, when interpreted deeply, encompasses all the interaction types that can be formed between the synthesized compounds and the adsorbent (hydrogen or van der Waals interactions). The electrochemical analysis is

confirmed by bonding interaction mechanisms using the topological parameters and NCI-RDG analysis. The results of QTAIM parameters are provided in Table 6. The QTAIM and the NCI graphs are plotted in Figure 17(a, b).

From Figure 17(a), it is shown that the  $\text{Zn}_4\text{O}_4\text{-glucose}$  (Cyc.) complex has a positive value of the Laplacian indicating the presence of non-covalent interactions. The electronic density values vary from 0.0600 to 0.0835 a.u. It is obtained a positive  $G(r)/\rho(r)$  ratio, the values are less than the unit. The calculated  $G(r)/\rho(r)$  ratio values confirmed the Laplacian sign results. It is demonstrated that  $\text{Zn}_4\text{O}_4$  (Cyc.) is able to detect glucose through a strong hydrogen bond formed between the O atom of the  $\text{Zn}_4\text{O}_4$  and the H atom of the glucose, with a value of approximately  $-62.74 \text{ kJ mol}^{-1}$  (BCP3). From the NCI index analysis, a blue spot is observed between these atoms, which explain that the glucose forms a strong hydrogen bonding interaction with the studied compounds. It is shown that the BCP3 specified by a lower ellipticity value equal to 0.01 a.u. justifies the stability of this interaction. The interplay of the glucose with the  $\text{Zn}_4\text{O}_4$  (W) molecule forms clearly two interactions bonds. The

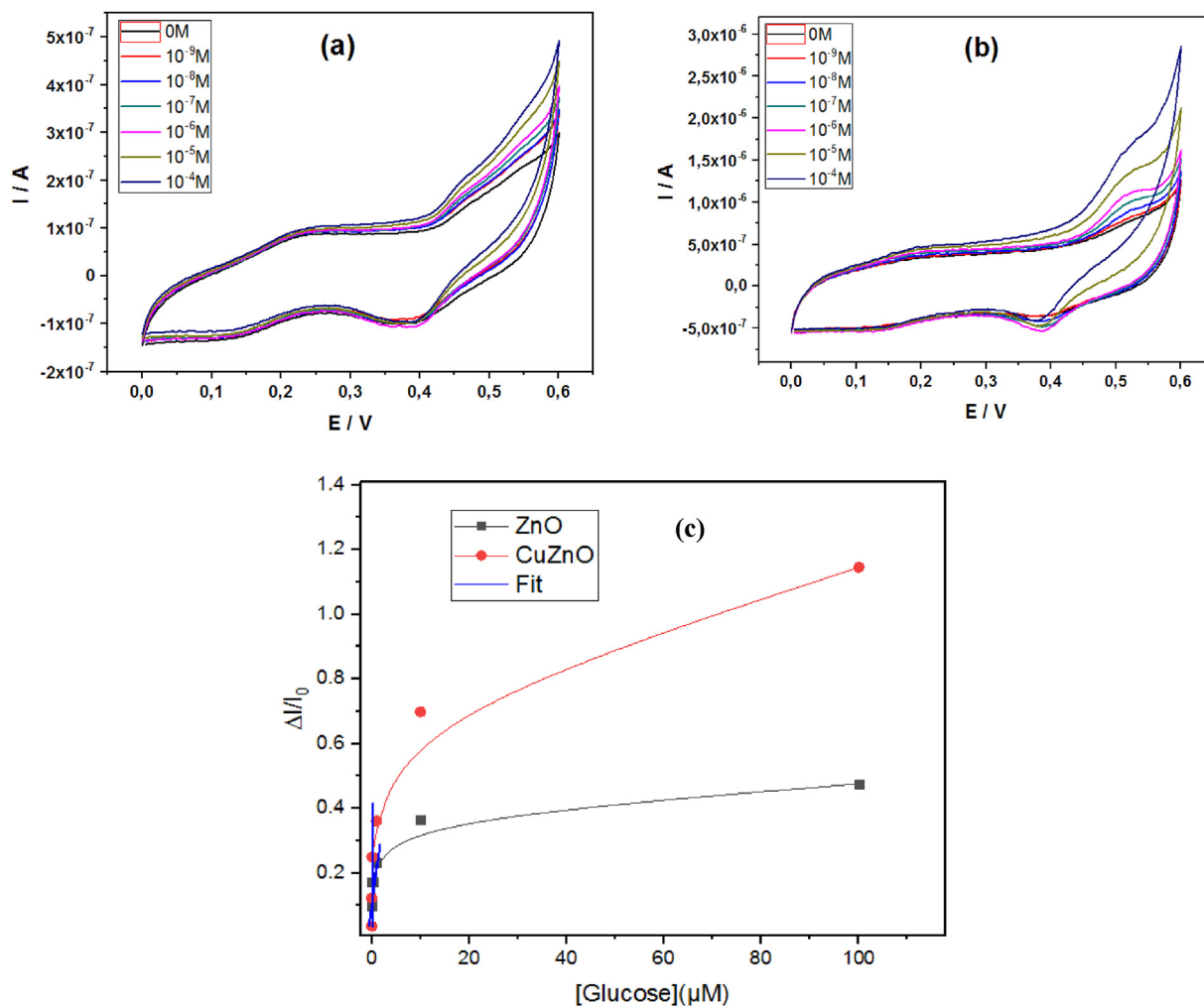
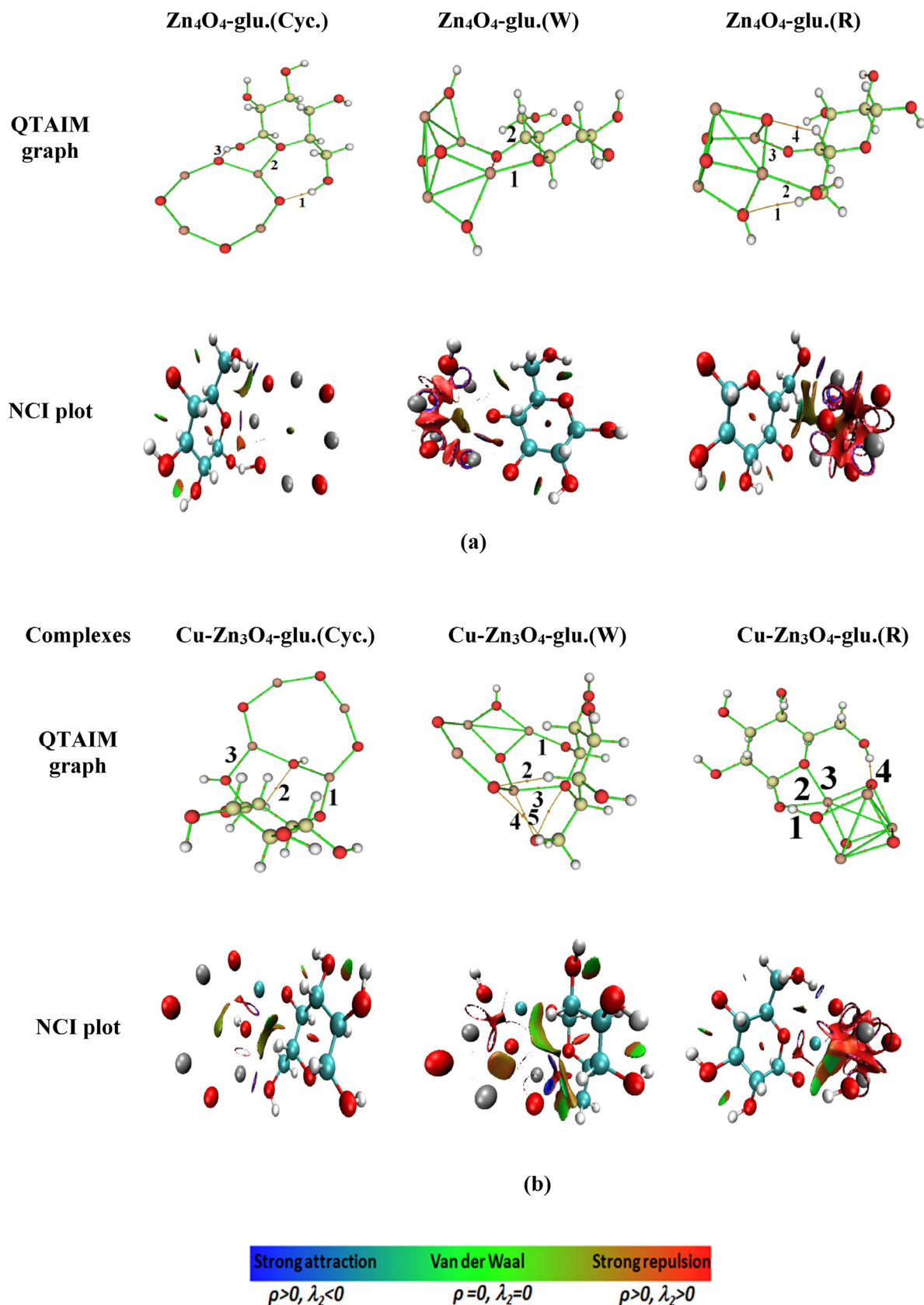


Figure 16. Electrochemistry characterization of ZnO and Cu-ZnO in the presence of increasing concentrations of glucose.

Table 6. The topological parameters (in a.u.): Electron density  $\rho(r)$ , Laplacian of electron density  $\nabla^2\rho(r)$ , Lagrangian kinetic energy density  $G(r)$ , potential energy density  $V(r)$ , ellipticity of electron density  $\varepsilon(r)$ , and the estimated interaction energy  $E_{H\cdots O}$  in  $\text{kJ}\cdot\text{mol}^{-1}$  at the selected BCPs.

Complexes	BCP	$\rho(r)$	$\nabla^2\rho(r)$	$G(r)$	$G(r)/\rho(r)$	$V(r)$	$\varepsilon(r)$	$E_{H\cdots O}$
Zn <sub>4</sub> O <sub>4</sub> -Glu	1	0.0600	0.1809	0.0535	0.89	-0.0617	0.007	-21.52
	2	0.0659	0.3821	0.0854	1.29	-0.0957	0.08	-26.25
	3	0.0835	0.1783	0.0684	0.81	-0.0923	0.01	-62.74
Zn <sub>4</sub> O <sub>4</sub> -Glu (W)	1	0.0913	0.5326	0.1178	1.29	-0.5326	0.08	-47.78
	2	0.2232	-0.3214	0.1360	0.60	-0.3524	0.01	-551.35
Zn <sub>4</sub> O <sub>4</sub> -Glu (R)	1	0.0126	0.0493	0.0104	0.82	-0.0085	0.16	4.98
	2	0.0573	0.3073	0.0705	1.23	-0.0797	0.06	-23.89
	3	0.0915	0.5525	0.1209	1.32	-0.0172	0.06	-45.15
	4	0.0236	0.0963	0.0216	0.91	-0.0201	0.04	3.93
Cu-Zn <sub>3</sub> O <sub>4</sub> -Glu	1	0.0984	0.6774	0.1847	1.87	-0.2000	0.04	-39.38
	2	0.0127	0.0558	0.0114	0.89	-0.0089	0.17	6.30
	3	0.0655	0.3819	0.0849	1.25	-0.0949	0.06	-26.25
Cu-Zn <sub>3</sub> O <sub>4</sub> -Glu(W)	1	0.1029	0.6740	0.1871	1.81	-0.2058	0.04	-48.83
	2	0.0200	0.0751	0.0172	0.86	-0.0156	0.05	3.93
	3	0.0523	0.2578	0.0616	1.17	-0.0711	0.07	-24.67
	4	0.0236	0.1286	0.0277	1.17	-0.0232	1.59	11.55
	5	0.2185	-0.4079	0.5300	2.42	-0.2079	0.08	-404.32
Cu-Zn <sub>3</sub> O <sub>4</sub> -Glu (R)	1	0.3130	-0.0138	0.0629	2.00	-0.4721	0.007	-750.22
	2	0.0727	0.4581	0.1163	1.59	-0.1182	0.07	-4.83
	3	0.0647	0.4685	0.1148	1.77	-0.1125	0.06	5.77
	4	0.0618	0.1858	0.0555	0.89	-0.0645	0.01	-23.62



**Figure 17.** QTAIM molecular graphs and NCI-RDG iso-surfaces of the most stable complexes. (a) (ZnO)<sub>4</sub>-glucose (Cyc., R, and W), and (b) Cu-Zn<sub>3</sub>O<sub>4</sub>-glucose (Cyc., R, and W). W: Wurtzite and R: Rocksalt are the cyclic forms.

strong hydrogen bonding interaction in the  $Zn_4O_4$ -glucose (W) complex is characterized by a higher electronic density (BCP2) than that of BCP3. In the BCP2, a negative value of  $\nabla^2\rho(r) = -0.3214$  a.u. is observed. This result indicated that an ionic interaction is formed between the two systems. It is found that  $Zn_4O_4$  (W) is bonded with the glucose by a strong hydrogen bonding equal to an interaction energy of  $-551.35$  kJ mol<sup>-1</sup>. The strong hydrogen bonding interaction formed between the  $Zn_{28}$  atom of W and the  $O_3$  of glucose is shown with blue spots in the NCI graph (see Figure 17(a)). The low value of the ellipticity (0.01 a.u.) for this bond indicates the stability of this interaction.

It can be concluded that the Wurtzite shape is more suitable to adsorb glucose than the cyclic form. Before doping; the rocksalt structure is stabilized by four interactions, two hydrogen bonds and two van der Waals interactions. From Table 6, it is shown that the  $Zn_4O_4$ -glucose (R) is characterized by its electronic density, ranging from 0.0126 to 0.0915 a.u. Positive values of the Laplacian indicate the presence of non-covalent interactions between the two systems. BCP1 and BCP4 are specified by van der Waals interactions. These low and strong interactions that favor the adsorption of glucose by the R shape are indicated in green (van der Waals forces) and blue spots (hydrogen forces) (see NCI index plot). The BCP3 is characterized by its interaction energy of  $-45.15$  kJ mol<sup>-1</sup>. These findings concluded that the glucose entity is well adsorbed via Rocksalt shape. After doping, the topological parameters and the visualization of the interaction forces formed between glucose and the title compounds were performed with a comparison of adsorption efficiency before Cu doping. From Table 6, it is shown that the electronic density of the Cu- $Zn_4O_4$ -glucose (Cyc.) complex varies from 0.0127 a.u. to 0.0984 a.u. Positive values of  $\nabla^2\rho(r)$  were found. This result indicated the presence of a covalent bond formed between the two systems. In the BCP1, the  $G(r)/\rho(r)$  ratio is equal to 1.87 a.u., explaining that the interaction between  $Cu_{32}$  and  $O_2$  is of the covalent type. It is characterized by a high interaction energy of  $-39.38$  a.u. Also, the Cu- $Zn_4O_4$  is bonded with glucose by other hydrogen forces localized between the  $Zn_{23}$  of the cyclic shape and the  $O_6$  of the guest (Figure 17 (b)). These results are confirmed by the 3D NCI Figures, where a blue spot appears in the BCP1 and BCP3. All these findings show that this synthesized compound is adequate for glucose adsorption. In the comparison between the two doped complexes,  $Zn_4O_4$  (W) and  $Zn_4O_4$  (R), it is clearly obtained that these two complexes are detecting glucose by strong hydrogen and weak van der Waals interactions. The Cu-W-glucose complex shows strong hydrogen bonding interactions formed between the  $Cu_{32}$  (W) and  $O_5$  (glucose). This interaction specified by  $E_{H...O}$  energy is equal to  $-48.83$  kJ mol<sup>-1</sup>. The second hydrogen bonding interaction coexists between  $Zn_{31}$  (W) and  $O_1$  (glucose). The value of this bonding is  $-404.32$  kJ mol<sup>-1</sup> of interaction energy. Also, a green spot in the BCP2 and BCP4 confirmed the presence of van der Waals interactions. In addition, in the BCP5, the  $G(r)/\rho(r)$  ratio is bigger than the unit ( $G(r)/\rho(r) = 2.42$  a.u. > 1). This result indicates that this interaction is a covalent bond. Concerning the  $Zn_4O_4$  (R), it is obtained that the cluster bond with the glucose by a strong hydrogen bonding has an interaction energy of  $-750.22$  a.u. located between the  $H_{23}$  of glucose and  $O_{25}$  of R. In this complex, for the BCP1, it is found to have a low ellipticity of electron density, which confirms a high chemical stability from this interaction. Also, the cation Cu is interacting with the O atom of glucose via van der Waals interactions. It shows the formation of hydrogen bonding between  $O_{30}$  (R) and  $H_{24}$  (glucose). It is concluded that the R shape adsorbed the glucose via hydrogen bond interaction.

Finally, a deeply QTAIM-NCI analysis concluded that the doped Cu enhanced the detection and adsorption of glucose by  $Zn_{n-1}O_n$  clusters. The results are well confirmed by the electrochemistry characterization. It is found that the doped Cu-Rocksalt is very suitable for the detection of glucose.

## 5. Conclusion

The computational DFT-D3 has been used to relax all the possible conformations of the  $Zn_nO_n$ , Cu- $(Zn_{n-1}O_n)$ ,  $(Zn_nO_n)$ -glucose, and Cu-

$(Zn_{n-1}O_n)$ -glucose complexes. The TEM and XRD characterizations of the ZnO and Cu-ZnO compounds have been experimentally interpreted. The investigation of the chemical properties and the charge transfer between the stable clusters and glucose using frontiers molecular orbital and MEP isosurfaces aided in the prediction of the mechanism of adsorption of the glucose guest. The sensibility of Cu- $(Zn_{n-1}O_n)$  to the glucose has been discussed in terms of the electrophilicity or nucleophilicity behavior of the cluster. A through infrared study was done for the most stable complexes, confirming the dynamic stability of the title compounds. The chemical reactivity and the active acceptor sites for the glucose in the studied clusters are deeply discussed. Energetically, it is demonstrated that the doping compounds Cu- $(Zn_3O_4)$ -glucose, Cu-Wurtzite-glucose, and Cu-Rocksalt-glucose are very suitable for adsorbing and detecting the glucose entity. The theoretical results are well confirmed by an experimental electrochemical analysis. The QTAIM and NCI-RDG analyses have demonstrated that the glucose adsorption is done by strong hydrogen bonds.

## Declarations

### Author contribution statement

B. Gassoumi: Analyzed and interpreted the data; Wrote the paper.  
 N. Aouled Dlala, M. E. Castro, F.J. Melendez, H. Ghalla, N. Leila, F. Madi, R. Ben Chaabane: Analyzed and interpreted the data.  
 M. Echabaane: Conceived and designed the experiments; Performed the experiments; Contributed reagents, materials, analysis tools or data.  
 A. Karayel, S. Özkinalı: Conceived and designed the experiments; Contributed reagents, materials, analysis tools or data.

### Funding statement

This work was supported by Tunisian's Ministry of high education and scientific research.

### Data availability statement

Data included in article/supplementary material/referenced in article.

### Declaration of interests statement

The authors declare no conflict of interest.

### Additional information

Supplementary content related to this article has been published online at <https://doi.org/10.1016/j.heliyon.2022.e12387>.

## References

- [1] V. Wagner, A. Dullaart, A.-K. Bock, A. Zweck, The emerging nanomedicine landscape, *Nat. Biotechnol.* 24 (2006) 1211–1217.
- [2] M. Ferrari, Cancer nanotechnology: opportunities and challenges, *Nat. Rev. Cancer* 5 (2005) 161–171.
- [3] T. Lammers, F. Kiessling, M. Ashford, W. Hennink, D. Crommelin, G. Storm, Erratum: cancer nanomedicine: is targeting our target? *Nat. Rev. Mater.* 1 (2016) 1–2.
- [4] H. Xiang, L. Zhao, L. Yu, H. Chen, C. Wei, Y. Chen, Y. Zhao, Self-assembled organic nanomedicine enables ultrastable photo-to-heat converting theranostics in the second near-infrared biowindow, *Nat. Commun.* 12 (2021) 218.
- [5] R. Rajamohan, S. Ashokkumar, Y.R. Lee, Environmental free synthesis of biologically active Cu<sub>2</sub>O nanoparticles for the cytotoxicity, *J. Mol. Struct.* 1271 (2022), 134081.
- [6] Z. Cheng, Y. Li, K. Wang, X. Zhu, P. Tharkar, W. Shu, T. Zhang, S. Zeng, L. Zhu, M. Murray, W. Chrzanowski, F. Zhou, Compritol solid lipid nanoparticle formulations enhance the protective effect of betulinic acid derivatives in human Müller cells against oxidative injury, *Exp. Eye Res.* 215 (2022) 108906.
- [7] N.N. Farshori, M.M. Al-Oqail, E.S. Al-Sheddi, S.M. Al-Massarani, Q. Saquib, M.A. Siddiqui, R. Wahab, A.A. Al-Khedhairi, Green synthesis of silver nanoparticles

- using Phoenix dactylifera seed extract and its anticancer effect against human lung adenocarcinoma cells, *J. Drug Delivery Sci. Technol.* 70 (2022), 103260.
- [8] P. Prema, T. Boobalan, A. Arun, K. Rameshkumar, R. Suresh Babu, V. Veeramaniandan, V.-H. Nguyen, P. Balaji, Green tea extract mediated biogenic synthesis of gold nanoparticles with potent anti-proliferative effect against PC-3 human prostate cancer cells, *Mater. Lett.* 306 (2022), 130882.
- [9] I. Rajendran, T. Ponrasu, R. Rajaram, L. Suguna, The apoptotic effect of Ferulic acid-synthesized gold nanoparticles against human epidermoid carcinoma (A431) cells via activation of caspase-3 pathway, *J. Drug Deliv. Sci. Technol.* 63 (2021), 102478.
- [10] S. Nasraoui, N. Ben Brahim, N. Bel Haj Mohamed, R. Ben Chaabane, A.R. Allouche, Theoretical and experimental investigation on ligands-CdS clusters interactions: Influence of solvent, *J. Mol. Struct.* 1173 (2018) 894–902.
- [11] S. Nasraoui, G. Attia, N.B. Haj Mohamed, R. Ben Chaabane, A.R. Allouche, Effects of thiol ligands on the growth and stability of CdS nanoclusters, *J. Mol. Struct.* 1198 (2019), 126832.
- [12] C. Sun, C. Zhang, B. Zhang, Adjusting the structural, electronic and optical properties of CdS by the introduction of Be: a DFT study, *Mater. Today Commun.* 31 (2022), 103394.
- [13] S. Dhar, B. Sen, S.K. Mukhopadhyay, T. Mukherjee, A.P. Chattopadhyay, S. Pramanik, CdS quantum dots embedded in PVP: Inorganic phosphate ion sensing in real sample and its antimicrobial activity, *Spectrochim. Acta Mol. Biomol. Spectrosc.* 234 (2020), 118256.
- [14] A.M. Abdelghany, E.M. Abdelrazek, D.S. Rashad, Impact of in situ preparation of CdS filled PVP nano-composite, *Spectrochim. Acta Mol. Biomol. Spectrosc.* 130 (2014) 302–308.
- [15] M.E. Khan, A. Mohammad, W. Ali, A.U. Khan, W. Hazmi, W. Zakri, T. Yoon, Excellent visible-light photocatalytic activity towards the degradation of tetracycline antibiotic and electrochemical sensing of hydrazine by SnO<sub>2</sub>-CdS nanostructures, *J. Clean. Prod.* 349 (2022), 131249.
- [16] M. Piotrowski, J. Borne, E. Carbó-Arribay, D. Sharma, N. Nicora, S. Sadewasser, D.Y. Petrovykh, C. Rodríguez-Abreu, Y.V. Kolen'ko, Template-directed self-organization of colloidal PbTe nanocrystals into pillars, conformal coatings, and self-supported membranes, *Nanoscale Adv.* 1 (2019) 3049–3055.
- [17] H. Zhang, M. Liu, T. Zhou, B. Dong, C.Y. Li, Stepwise assembly of a cross-linked free-standing nanoparticle sheet with controllable shape, *Nanoscale* 7 (2015) 11033–11039.
- [18] I. Elahi, S.M. Alay-e-Abbas, S. Nazir, G. Abbas, W. Akbar, A. Shaukat, M.N. Tahir, Formation energetics, electronic structure and Ferromagnetic properties of C-, Si- and Ge-doped zinc Blende Cadmium Chalcogenides, *Mater. Today Commun.* 25 (2020), 101652.
- [19] K.T. Chavan, S. Chandra, A. Kshirsagar, Half-metallicity in smallest cage-like cluster of CdTe with doping of transition metal atoms, *Mater. Today Commun.* 30 (2022), 103104.
- [20] Ü. Özgür, V. Avrutin, H. Morkoç, Chapter 16 – zinc oxide materials and devices grown by molecular beam epitaxy, in: M. Henini (Ed.), *Molecular Beam Epitaxy*, second ed., Elsevier, 2018, pp. 343–375.
- [21] W.L. de Almeida, F.S. Rodembusch, N.S. Ferreira, V. Caldas de Sousa, Eco-friendly and cost-effective synthesis of ZnO nanopowders by Tapioca-assisted sol-gel route, *Ceram. Int.* 46 (2020) 10835–10842.
- [22] F. Ameen, T. Dawoud, S. AlNadhari, Ecofriendly and low-cost synthesis of ZnO nanoparticles from Acremonium protionii for the photocatalytic degradation of azo dyes, *Environ. Res.* 202 (2021), 111700.
- [23] H.-C. Wang, Y. Hong, Z. Chen, C. Lao, Y. Lu, Z. Yang, Y. Zhu, X. Liu, ZnO UV photodetectors modified by Ag nanoparticles using all-Inkjet-Printing, *Nanoscale Res. Lett.* 15 (2020) 176.
- [24] C. Jayaseelan, A.A. Rahuman, A.V. Kirthi, S. Marimuthu, T. Santhoshkumar, A. Bagavan, K. Gaurav, L. Karthik, K.V.B. Rao, Novel microbial route to synthesize ZnO nanoparticles using *Aeromonas hydrophila* and their activity against pathogenic bacteria and fungi, *Spectrochim. Acta Mol. Biomol. Spectrosc.* 90 (2012) 78–84.
- [25] A. Tamvakos, K. Korir, D. Tamvakos, D. Caletani, G. Cicero, D. Pullini, NO<sub>2</sub> gas sensing mechanism of ZnO thin-film transducers: physical experiment and theoretical correlation study, *ACS Sens.* 1 (2016) 406–412.
- [26] V.D. Mote, Y. Purushotham, B.N. Dole, Structural, morphological, physical and dielectric properties of Mn doped ZnO nanocrystals synthesized by sol-gel method, *Mater. Des.* 96 (2016) 99–105.
- [27] W.-J. Wu, Q. Zhao, R. Zhou, Y.-C. Liang, W.-B. Zhao, C.-X. Shan, Ratiometric fluorescence sensor based on europium-grafted ZnO quantum dots for visual and colorimetric detection of tetracycline, *Spectrochim. Acta Mol. Biomol. Spectrosc.* 259 (2021) 119901.
- [28] A.A. Ensafi, M. Zakery, B. Rezaei, An optical sensor with specific binding sites for the detection of thioridazine hydrochloride based on ZnO-QDs coated with molecularly imprinted polymer, *Spectrochim. Acta Mol. Biomol. Spectrosc.* 206 (2019) 460–465.
- [29] T. Pandiyarajan, R.V. Mangalaraja, B. Karthikeyan, R. Udayabhaskar, D. Contreras, S. Sepulveda-Guzman, M.A. Gracia-Pinilla, Influence of RE (Pr<sup>3+</sup>, Er<sup>3+</sup>, Nd<sup>3+</sup>) doping on structural, vibrational and enhanced persistent photocatalytic properties of ZnO nanostructures, *Spectrochim. Acta Mol. Biomol. Spectrosc.* 268 (2022) 120679.
- [30] S.P. Tiwari, M.K. Mahata, K. Kumar, V.K. Rai, Enhanced temperature sensing response of upconversion luminescence in ZnO-CaTiO<sub>3</sub>: Er<sup>3+</sup>/Yb<sup>3+</sup> nano-composite phosphor, *Spectrochim. Acta Mol. Biomol. Spectrosc.* 150 (2015) 623–630.
- [31] M.H. Hassan, C. Vyas, B. Grieve, P. Bartolo, Recent advances in enzymatic and non-enzymatic electrochemical glucose sensing, *Sensors* 21 (2021) 4672.
- [32] N.A. Yoon, S. Diano, Hypothalamic glucose-sensing mechanisms, *Diabetologia* 64 (2021) 985–993.
- [33] S.M. Mousavi, S.A. Hashemi, A. Gholami, S. Mazraeidoost, W.-H. Chiang, O. Arjmand, N. Omidifar, A. Babapour, Precise blood glucose sensing by nitrogen-doped graphene quantum dots for Tight Control of Diabetes, *J. Sens.* 2021 (2021), e5580203.
- [34] W.-C. Lee, E.H. Koh, D.-H. Kim, S.-G. Park, H.S. Jung, Plasmonic contact lens materials for glucose sensing in human tears, *Sens. Actuat. B: Chem.* 344 (2021), 130297.
- [35] H. Ullah, R. Ahmad, A.A. Khan, N. Khaliq, M. Khan, G. Ali, S. Karim, X. Yi, S.O. Cho, A sensitive non-enzymatic glucose sensor based on MgO entangled nanosheets decorated with CdS nanoparticles: experimental and DFT study, *J. Mol. Liq.* 360 (2022) 119366.
- [36] P. Lakhera, S. Singh, R. Mehla, V. Chaudhary, P. Kumar, S. Kumar, Boronic acid decorated graphene nano flakes for glucose sensing in diabetes: a DFT prediction, *IEEE Sensor. J.* 22 (2022) 7572–7579.
- [37] F. Saira, A. Yaqub, H. Razaq, M.G. Sohail, S. Saleemi, M. Mumtaz, M.A. Rafiq, S. Qaisar, Hollow nanocages for electrochemical glucose sensing: a comprehensive review, *J. Mol. Struct.* 1268 (2022), 133646.
- [38] K. Omri, I. Najeh, L. El Mir, Influence of annealing temperature on the microstructure and dielectric properties of ZnO nanoparticles, *Ceram. Int.* 42 (2016) 8940–8948.
- [39] S. Grimme, Semiempirical hybrid density functional with perturbative secondorder correlation, *J. Chem. Phys.* 124 (2006), 034108.
- [40] S. Grimme, J. Antony, S. Ehrlich, H. Krieg, A consistent and accurate ab initio parametrization of density functional dispersion correction (DFT-D) for the 94elements, *J. Chem. Phys.* 132 (2010), 154104.
- [41] M.J. Frisch, W.G. Trucks, H.B. Schlegel, G.E. Scuseria, M.A. Robb, J.R. Cheeseman, G. Scalmani, V. Barone, B. Mennucci, G.A. Petersson, H. Nakatsuji, M. Caricato, X. Li, H.P. Hratchian, A.F. Izmaylov, J. Bloino, G. Zheng, J.L. Sonnenberg, M. Hada, M. Ehara, K. Toyota, R. Fukuda, J. Hasegawa, M. Ishida, T. Nakajima, Y. Honda, O. Kitao, H. Nakai, T. Vreven, J.A. Montgomery Jr., J.E. Peralta, F. Ogliaro, M. Bearpark, J.J. Heyd, E. Brothers, K.N. Kudin, V.N. Staroverov, T. Keith, R. Kobayashi, J. Normand, K. Raghavachari, A. Rendell, J.C. Burant, S.S. Iyengar, J. Tomasi, M. Cossi, N. Rega, J.M. Millam, M. Klene, J.E. Knox, J.B. Cross, V. Bakken, C. Adamo, J. Jaramillo, R. Gomperts, R.E. Stratmann, O. Yazyev, A.J. Austin, R. Cammi, C. Pomelli, J.W. Ochterski, R.L. Martin, K. Morokuma, V.G. Zakrzewski, G.A. Voth, P. Salvador, J.J. Dannenberg, S. Dapprich, A.D. Daniels, O. Farkas, J.B. Foresman, J.V. Ortiz, J. Cioslowski, D.J. Fox, Gaussian 09, Gaussian, Inc., Wallingford CT, 2010.
- [42] D. Roy, K. Todd, M. John, GaussView. Version 5, Semichem Inc. Shawnee Mission, KS, 2009.
- [43] C. Lee, W. Yang, R.G. Parr, Development of the Colle-Salvetti correlation-energy formula into a functional of the electron density, *Phys. Rev. B* 37 (1988) 785–789.
- [44] P.J. Hay, W.R. Wadt, Ab initio effective core potentials for molecular calculations. Potentials for the transition metal atoms Sc to Hg, *J. Chem. Phys.* 82 (1985) 270–283.
- [45] R.F.W. Bader, *Atoms in Molecules: A Quantum Theory*, Oxford University Press, Oxford, New York, 1994.
- [46] T. Lu, F. Chen, Multiwfn: a multifunctional wavefunction analyzer, *J. Comput. Chem.* 33 (2012) 580–592.
- [47] V.L. Chandraboss, B. Karthikeyan, S. Senthilvelan, Experimental and first-principles study of guanine adsorption on ZnO clusters, *Phys. Chem. Chem. Phys.* 16 (2014) 23461–23475.
- [48] S. Dheivamalar, K.B. Banu, A DFT study on functionalization of acrolein on Ni-doped (ZnO)<sub>6</sub> nanocluster in dye-sensitized solar cells, *Heliyon* 5 (2019), e02903.
- [49] S. Shou-heng, S. Chuan, K. Fink, V. Staemmler, An ab initio study of the adsorption of CO on a Zn<sub>4</sub>O<sub>4</sub> cluster with wurtzite-like structure, *Chem. Phys.* 287 (2003) 183–195.
- [50] S.B. Woodley, A.A. Sokol, C.R.A. Catlow, A.A. Al-Sunaidi, S.M. Woodley, Structural and optical properties of Mg and Cd doped ZnO nanoclusters, *J. Phys. Chem. C* 117 (2013) 27127–27145.
- [51] A.A. Devi, S. Vidy, P.K. Rai, B.G. Jeyaprakash, Theoretical investigation of H<sub>2</sub> interactions on ZnO cluster: DFT approach, *Int. J. Nanosci.* 17 (2018), 1760041.
- [52] N. Tayade, S.M. Mane, M.P. Tirpude, J.C. Shin, Perspective of Zn<sub>3</sub>O<sub>3</sub> ring cluster via density functional theory, *Mater. Today Commun.* 27 (2021), 102343.
- [53] R. Stuedel, Y. Stuedel, Interaction of zinc oxide clusters with molecules related to the Sulfur Vulcanization of Polyolefins (“Rubber”), *Chem. Eur. J.* 12 (2006) 8589–8602.
- [54] P.D.J. Grootenhuis, P.A. Kollman, L.C. Groenen, D.N. Reinhoudt, G.J. Hummel, F. Ugozzoli, G.D. Andreotti, Computational study of the structural, energetical, and acid-Base properties of calix[4]arenes, *J. Am. Chem. Soc.* 112 (1990) 4165–4176.
- [55] S. Özkınalı, Spectroscopic and thermal properties of newly mixed azocalix[4]arene ester derivatives, *Dyes Pigments* 107 (2014) 81–89.
- [56] A. Zając, L. Dymińska, J. Lorenc, S.M. Kaczmarek, G. Leniec, M. Ptak, J. Hanuza, Spectroscopic properties and molecular structure of copper phytate complexes: IR, Raman, UV-Vis, EPR studies and DFT calculations, *J. Biol. Inorg. Chem.* 24 (2019) 11–20.
- [57] B. Gassoumi, F.E. Ben Mohamed, M.E. Castro, F.J. Melendez, A. Karayel, L. Nour, F. Madi, H. Ghalla, S. Özkınalı, V.I. Kovalenko, R. Ben Chaabane, H. Ben Ouada, In silico exploration of O-H...X<sub>2</sub>+ (X = Cu, Ag, Hg) interaction, targeted adsorption zone, charge density iso-surface, O-H proton analysis and topographic parameters theory for calix[6]arene and calix[8]arene as model, *J. Mol. Liq.* 334 (2021), 116127.

- [58] X. Wang, M. Deng, Z. Zhao, Q. Zhang, Y. Wang, Synthesis of super-hydrophobic CuO/ZnO layered composite nano-photocatalyst, *Mater. Chem. Phys.* 276 (2022), 125305.
- [59] A. Bhattacharyya, S. Sen, K. Harms, S. Chattopadhyay, Formation of three photoluminescent zinc(II) complexes with Zn2O2 cores: examples of bi-dentate bonding modes of potentially tri- and tetra-dentate Schiff bases, *Polyhedron* 88 (2015) 156–163.
- [60] A. Escobedo-Morales, R. Esparza, A. García-Ruiz, A. Aguilar, E. Rubio-Rosas, R. Pérez, Structural and vibrational properties of hydrothermally grown ZnO nanoparticles, *J. Cryst. Growth* 316 (2011) 37–41.
- [61] S. Özkınalı, Ş. Yavuz, T. Tosun, D. Ali Köse, M. Gür, H. Kocaokutgen, Synthesis, spectroscopic and thermal analysis and investigation of dyeing properties of *o*-hydroxy schiff bases and their metal complexes, *ChemistrySelect* 5 (2020) 12624–12634.
- [62] I.-P. Zaragoza, L.-A. Soriano-Agueda, R. Hernández-Esparza, R. Vargas, J. Garza, Analyzing ZnO clusters through the density-functional theory, *J. Mol. Model.* 24 (2018) 164.
- [63] Investigations on 2-(4-Cyanophenylamino) acetic acid by FT-IR, FT-Raman, NMR and UV-Vis spectroscopy, DFT (NBO, HOMO-LUMO, MEP and Fukui function) and molecular docking studies, *Heliyon* 6 (2020), e04976.
- [64] S. Sevvanthi, S. Muthu, M. Raja, S. Aayisha, S. Janani, PES, molecular structure, spectroscopic (FT-IR, FT-Raman), electronic (UV-Vis, HOMO-LUMO), quantum chemical and biological (docking) studies on a potent membrane permeable inhibitor: dibenzoxepine derivative, *Heliyon* 6 (2020), e04724.
- [65] M. Zangeneh Soroush, K. Maghooli, S.K. Setarehdan, A.M. Nasrabadi, Emotion recognition using EEG phase space dynamics and Poincare intersections, *Biomed. Signal Process Control* 59 (2020), 101918.
- [66] C. Tiwari, S.S. Jha, R. Kumar, M. Chhabra, B.D. Malhotra, A. Dixit, Exfoliated graphite carbon paper-based flexible nonenzymatic glucose sensor, *Mater. Sci. Eng., B* 285 (2022), 115931.
- [67] A.K. Shukla, A.P. Chaudhary, J. Pandey, Synthesis, spectral analysis, molecular docking and DFT studies of 3-(2, 6-dichlorophenyl)-acrylamide and its dimer through QTAIM approach, *Heliyon* 6 (2020), e05016.
- [68] A. Morales-Bayuelo, J. Sánchez-Márquez, Discerning the thermal cyclotrimerizations of fluoro- and chloroacetylenes through ELF, NBO descriptors and QTAIM analysis: pseudodiradical character, *Heliyon* 6 (2020), e04441.